CMS

CMS-HIG-21-013

Measurement of the Higgs boson width and evidence of its off-shell contributions to ZZ production

The CMS Collaboration*

Abstract

Since the discovery of the Higgs boson in 2012, detailed studies of its properties have been ongoing. Besides its mass, its width — related to its lifetime — is an important parameter. One way to determine this quantity is by measuring its off-shell production, where the Higgs boson mass is far away from its nominal value, and relating it to its on-shell production, where the mass is close to the nominal value. Here, we report evidence for such off-shell contributions to the production cross section of two Z bosons with data from the CMS experiment at the CERN Large Hadron Collider. We constrain the total rate of the off-shell Higgs boson contribution beyond the Z boson pair production threshold, relative to its standard model expectation, to the interval $[0.0061, 2.0]$ at 95% confidence level. The scenario with no off-shell contribution is excluded at a p-value of 0.0003 (3.6 standard deviations). We measure the width of the Higgs boson as $\Gamma_{\mathrm{H}} = 3.2^{+2.4}_{-1.7}$ MeV, in agreement with the standard model expectation of 4.1 MeV. In addition, we set constraints on anomalous Higgs boson couplings to W and Z boson pairs.

*See Appendix 1 for the list of collaboration members

The standard model (SM) of particle physics provides an elegant description for the masses and interactions of fundamental particles. These are fermions, which are the building blocks of ordinary matter, and gauge bosons, which are the carriers of the electroweak (EW) and strong forces. In addition, the SM postulates the existence of a quantum field responsible for the generation of the masses of fundamental particles through a phenomenon known as the Brout–Englert–Higgs mechanism. This field, known as the *Higgs field* [1–3], interacts with SM particles, giving them mass, as well as with itself. The field carrier is a massive, scalar (spin-0) particle known as the Higgs (H) boson. Nearly half a century after its postulation, it was finally observed in 2012 with a mass m_H of around $125\,\text{GeV}$ by the ATLAS and CMS Collaborations [4–6] at the CERN Large Hadron Collider (LHC). Given the unique role the H boson plays in the SM, studies of its properties are a major goal of particle physics.

Apart from mass, another important property of a particle is its lifetime τ. Only a few fundamental particles are stable; others—including the H boson—exist only for a fleeting moment before disintegrating into other, lighter, species. The Heisenberg uncertainty principle [7] provides a direct connection between the lifetime of a particle and the uncertainty in its mass, a property known as the particle's width, Γ. Any unstable particle (often referred to as a *resonance*) has a finite lifetime, with shorter τ corresponding to broader Γ. The two quantities are related through the Planck constant, h, as $\Gamma = h/(2\pi\tau)$. Even with perfect experimental resolution, the observed mass of an unstable particle will not be constant across a series of measurements (e.g., of the invariant mass of its decay products i, which is calculated from the sums of their energies, E_i, and momenta, $\vec{p}_i$, as $\sqrt{(\sum_i E_i)^2 - |\sum_i \vec{p}_i|^2}$). The possible mass values are distributed according to a characteristic relativistic Breit–Wigner distribution [8] with a nominal mass value corresponding to the maximum of the Breit–Wigner, and with width parameter Γ.

Particles are understood to be *on the mass shell* (on-shell) if their mass is close to the nominal mass value, and *off-shell* if their mass takes a value far away from it. By the aforementioned property of the Breit–Wigner line shape, particles are generally more likely to be produced on-shell than off-shell when energy and momentum conservation allows it. Scattering amplitudes (A) for off-shell particle production, followed by a specific decay final state, may be modified further by interference with other processes, which is large and destructive in the case of the H boson. In this specific case, writing $A = H + C$, with H standing for the H boson contribution and C for other interfering contributions, we will use the term "off-shell production" as a shorthand for the $|H|^2$ term in $|A|^2$.

For broad resonances, the width can be obtained by directly measuring the Breit–Wigner line shape, e.g., as was done in the case of the Z boson, measured to have a mass of $m_Z = 91.188 \pm 0.002\,\text{GeV}$ and a width of $\Gamma_Z = 2.495 \pm 0.002\,\text{GeV}$ at the CERN Large Electron Positron collider [9]. The H boson is expected to live three orders of magnitude longer, with a theoretically predicted width of $\Gamma_H = 4.1\,\text{MeV}$ ($0.0041\,\text{GeV}$) [10], and a deviation from the SM prediction would indicate the existence of new physics. This width is too small to be measured directly from the line shape because of the limited mass resolution of order $1\,\text{GeV}$ achievable with the present LHC detectors. Another direct way of measuring the H boson width would be to measure its lifetime by means of its decay length and use the relationship $\Gamma_H = h/(2\pi\tau_H)$, but its lifetime is still too short ($\tau_H = 1.6 \times 10^{-22}\,\text{s}$) to be detectable directly. The present experimental limit on this quantity is $\tau_H < 1.9 \times 10^{-13}\,\text{s}$ at 95% confidence level (CL) [11], nine orders of magnitude above the SM lifetime.

The value of Γ_H can be extracted with much better precision through a combined measurement of on-shell and off-shell H boson production. In the decay of an H boson with $m_H \approx 125\,\text{GeV}$

to a pair of massive gauge bosons V (V = W or Z, with masses around 80.4 or 91.2 GeV, respectively), we have $m_V < m_H < 2m_V$. Therefore, when the H boson is produced on-shell (with the VV invariant mass $m_{VV} \sim m_H$), one of the V bosons must be off-shell to satisfy four-momentum conservation. Once the H boson is produced off-shell with large enough invariant mass $m_{VV} > 2m_V$ (off-shell H boson production region), the V bosons themselves are produced on-shell. Since the Breit–Wigner mass distribution of either the H or V boson maximizes at their respective nominal masses, the rate of off-shell H boson production above the V boson pair production threshold is enhanced with respect to what one would expect from the Breit–Wigner line shape of the H boson alone.

The measurement of the higher part of the m_{VV} spectrum can then be used to establish off-shell H boson production. The ratio of off-shell to on-shell production rates allows for a measurement of Γ_H [12, 13] via the cross section proportionality relations

$$\sigma^{\text{on-shell}} \propto \frac{g_p^2 g_d^2}{\Gamma_H} \propto \mu_p \Rightarrow \sigma^{\text{off-shell}} \propto g_p^2 g_d^2 \propto \mu_p \Gamma_H,$$

where g_p and g_d are the couplings associated with the H boson production and decay modes, respectively, and μ_p is the on-shell H boson signal strength in the production mode being considered. Each signal strength is defined as the ratio of the H boson squared amplitude in the measured cross section to that predicted in the SM. The off-shell H boson signal strength, $\mu_p^{\text{off-shell}}$, can be expressed as $\mu_p \Gamma_H$ in each production mode, and the scenario with no off-shell production becomes equivalent to the limiting case $\Gamma_H = 0$. For the rest of this article, we concentrate on the ZZ decay channel, i.e., g_d corresponding to the H → ZZ decay. The CMS and ATLAS Collaborations have previously used this method to set upper limits on Γ_H as low as 9.2 MeV at 95% CL [14, 15].

It is important to distinguish between two types of H boson production modes: the gluon fusion gg → H → ZZ process, where the H boson is produced via its couplings to fermions, and the EW processes, which involve HVV (i.e., HWW or HZZ) couplings. The top row of Fig. 1 shows the Feynman diagrams for the most dominant contributions to the gg (top left) process, and the EW processes of vector boson fusion (VBF, top center) and VH (top right). A more complete set of diagrams for the EW process are shown in Extended Data Figs. 1 and 2. Because different H boson couplings are involved in the gg and EW processes, we extract two off-shell signal strength parameters $\mu_F^{\text{off-shell}}$ for the gg mode and $\mu_V^{\text{off-shell}}$ for the EW mode. We also consider an overall off-shell signal strength parameter $\mu^{\text{off-shell}}$ with different assumptions on the ratio $R_{V,F}^{\text{off-shell}} = \mu_V^{\text{off-shell}} / \mu_F^{\text{off-shell}}$.

A major challenge arises from the fact that there are other sources of ZZ pairs in the SM (continuum ZZ production), see for example the bottom row of Fig. 1. These contributions, particularly those from $q\bar{q} \to ZZ$, are typically much larger than the contribution from off-shell H → ZZ. In addition, some of the amplitudes from continuum ZZ processes interfere with the H boson amplitudes because they share the same initial and final states. For example, the amplitudes in the first column of Fig. 1, or those in the second column, interfere with each other; the amplitude shown in the lower right panel (shown more generically in Extended Data Fig. 3) does not interfere with any of the other diagrams as we omit the negligible contribution of $q\bar{q} \to H \to ZZ$ that would interfere with it.

The interference between the H boson and continuum ZZ amplitudes is destructive [16–21]. This destructive interference plays a key role in the SM as it is one of the contributions that unitarizes the scattering of massive gauge bosons, keeping the computation of the cross section for ZZ production in proton-proton (pp) collisions finite [16–19]. Figure 2 displays the interplay

$gg \to H \to ZZ:$

$q_1q_2 \to q_1'q_2'H \to q_1'q_2'ZZ:$

$q\bar{q} \to ZH \to ZZZ:$

$gg \to ZZ:$

$q_1q_2 \to q_1'q_2'ZZ:$

$q\bar{q} \to ZZ:$
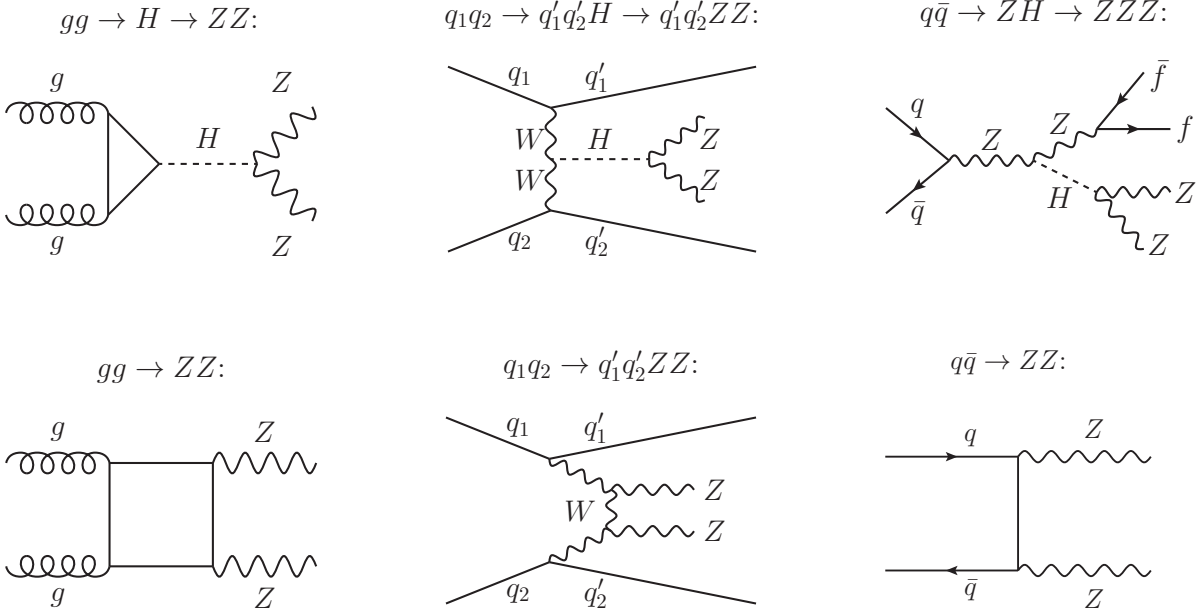
Figure 1: **Feynman diagrams for important contributions to ZZ production.** Diagrams can be distinguished as those involving the H boson (top), and those that give rise to continuum ZZ production (bottom). The interaction displayed at tree level in each diagram is meant to progress from left to right. Each straight, curvy, or curly line refers to the different set of particles denoted. Straight, solid lines with no arrows indicate the line could refer to either a particle or an antiparticle, whereas those with forward (backward) arrows refer to a particle (an antiparticle).

between the H boson production modes and the interfering continuum amplitudes, illustrating the growing importance of their destructive interference as m_{ZZ} grows in the two final states included in the analysis, $ZZ \to 2\ell2\nu$ and $ZZ \to 4\ell$. In the parametrization of the total cross section, contributions from this type of interference between the H boson and continuum ZZ amplitudes scale with $\sqrt{\mu_F^{\text{off-shell}}}$ and $\sqrt{\mu_V^{\text{off-shell}}}$ for the gg and EW modes, respectively.

In this article, we study off-shell H boson decays to $ZZ \to 2\ell2\nu$, and on-shell as well as off-shell H boson decays to $ZZ \to 4\ell$ ($\ell = \mu$ or e), using a sample of pp collisions at 13 TeV collected by the CMS experiment at the LHC. The selection and analysis of the off-shell $ZZ \to 2\ell2\nu$ data sample is described in detail in this article, and it is based on data collected between 2016 and 2018, corresponding to an integrated luminosity of 138 fb^{-1}. For the $ZZ \to 4\ell$ mode, we use previously published CMS off-shell (2016 and 2017 data sets, 78 fb^{-1} [15]) and on-shell (2015 [15, 22] and 2016–2018 [23] data sets, 2.3 fb^{-1} and 138 fb^{-1}, respectively) results.

Information on the off-shell signal strengths, Γ_H, and constraints on possible beyond-the-SM (BSM) anomalous couplings are extracted from combined fits over several kinematic distributions of the selected $2\ell2\nu$ and 4ℓ events. While off-shell events are the ones solely used to establish the presence of off-shell H boson production, the measurement of Γ_H relies on the combination of on-shell and off-shell data.

Because of the presence of neutrinos, the H boson mass cannot be precisely reconstructed in the H $\to 2\ell2\nu$ final state as the longitudinal component of the total momentum carrried by the neutrinos cannot be measured. Thus, on-shell information can only be extracted from the 4ℓ mode. This combination of 4ℓ and $2\ell2\nu$ data enables the measurement of Γ_H with a precision of ~50%. The measurement improves the upper limit on τ_H by eight orders of magnitude
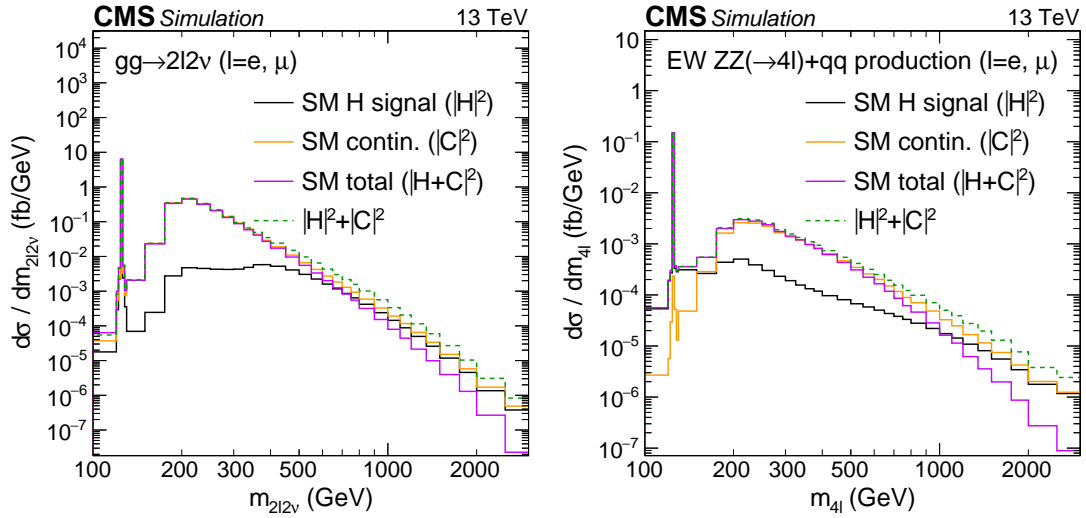
Figure 2: **Standard model calculations of ZZ invariant mass in the gg and EW processes.** Shown are the distributions for the $2\ell2\nu$ invariant mass, $m_{2\ell2\nu}$, from the $gg \to 2\ell2\nu$ process on the left panel, and the 4ℓ invariant mass, $m_{4\ell}$, from the EW $ZZ(\to 4\ell) + qq$ processes on the right. These processes involve the H boson ($|H|^2$) and interfering continuum ($|C|^2$) contributions to the scattering amplitude, shown in black and gold, respectively. The dashed green curve represents their direct sum without the interference ($|H|^2 + |C|^2$), and the solid magenta curve represents the sum with interference included ($|H + C|^2$). Note that the interference is destructive, and its importance grows as the mass increases. The integrated luminosity is taken to be $1\,\text{fb}^{-1}$, so these distributions are equivalent to the differential cross section spectra $d\sigma/dm_{2\ell2\nu}$ (left) and $d\sigma/dm_{4\ell}$ (right). The distributions are shown after requiring that all charged leptons satisfy $p_T > 7\,\text{GeV}$ and $|\eta| < 2.4$, and that the invariant mass of any charged lepton pair with same flavor and opposite charge is greater than $4\,\text{GeV}$. Here, p_T denotes the magnitude of the momentum of these leptons transverse to the pp collision axis, and η denotes their pseudorapidity, defined as $-\ln[\tan(\theta/2)]$ using the angle θ between their momentum vector and the collision axis. Calculations for the $gg \to 4\ell$ and EW $ZZ(\to 2\ell2\nu) + qq$ processes exhibit similar qualitative properties. The details of the Monte Carlo programs used for these calculations are given in the Methods section.

compared to the direct constraint from Ref. [11]. The inclusion of the $2\ell2\nu$ data also allows the lower limits on $\mu_V^{\text{off-shell}}$ to reach within $\sim$65% of its best fit value, compared to the weaker constraints from 4ℓ data alone, which reach within $\sim$90% of the 4ℓ-only best fit value [15].

The m_{ZZ} line shape is sensitive to the potential presence of anomalous HVV couplings [10, 11, 15, 24–26]. Thus, BSM physics could affect the ratio of off-shell to on-shell H boson production rates, and therefore the measurement of Γ_H. We test the effect of these couplings on the Γ_H measurement and constrain the contribution from these couplings themselves. In parametrizing anomalous HVV contributions, we adopt the formalism of Ref. [15] with the scattering amplitude

$$A \propto \left[a_1 - \frac{q_1^2 + q_2^2}{\Lambda_1^2}\right] m_V^2 \epsilon_1^* \epsilon_2^* + a_2 f_{\mu\nu}^{*(1)} f^{*(2)\,\mu\nu} + a_3 f_{\mu\nu}^{*(1)} \tilde{f}^{*(2)\,\mu\nu}.$$

Here, the polarization vector (four-momentum) of the vector boson V_i is denoted by ϵ_i (q_i) while $f^{(i)\mu\nu} = \epsilon_i^\mu q_i^\nu - \epsilon_i^\nu q_i^\mu$ and $\tilde{f}_{\mu\nu}^{(i)} = \frac{1}{2}\epsilon_{\mu\nu\rho\alpha} f^{(i)\,\rho\alpha}$ are tensor expressions for each V_i. The BSM couplings a_2, a_3, and $1/\Lambda_1^2$ (denoted generically as a_i) are assumed to be real and can take negative values, with the κ factors in Ref. [15] absorbed into the definition of $1/\Lambda_1^2$. The first two are coefficients for generic CP-conserving and CP-violating higher dimensional operators, respectively, while $1/\Lambda_1^2$ is the coefficient for the first-order term in the expansion of a SM-like tensor structure with an anomalous dipole form factor in the invariant masses of the two V bosons. In what follows, we will use the shorthand "a_i hypothesis" to refer to the scenario where all BSM HVV couplings other than a_i itself are zero.

Throughout this work, we assume that the gluon fusion loop amplitudes do not receive new physics contributions apart from a rescaling of the SM amplitude. Possible modifications of the m_{ZZ} line shape [26, 27] are neglected based on existing LHC constraints [28–30].

$2\ell2\nu$ analysis considerations

The $2\ell2\nu$ analysis is based on the reconstruction of $Z \to \ell\ell$ decays with a second Z boson decaying to neutrinos that escape detection. The momentum of the undetected Z boson transverse to the pp collision axis can be measured through an imbalance across all remaining particles, i.e., missing transverse momentum (p_T^{miss} or $\vec{p}_T^{\text{miss}}$ in vector form). Thus, the analysis requires large p_T^{miss} as the $Z \to \nu\nu$ signature.

The event selection is sensitive to the tail of the instrumental p_T^{miss} resolution in pp $\to$ Z+jets events that constitute an important reducible background. This contribution is estimated through a study of a data control region (CR) of γ+jets events, where p_T^{miss} is purely instrumental as it is in Z+jets events.

Processes such as pp $\to$ $t\bar{t}$ or WW result in nonresonant dilepton final states of same (e^+e^- and $\mu^+\mu^-$) and opposite flavor ($e^\pm\mu^\mp$) with the same probability and the same kinematic properties. Thus, their background contribution to the $2\ell2\nu$ signal, which includes two leptons of the same flavor, is estimated from an opposite-flavor $e\mu$ CR.

Other backgrounds from $q\bar{q} \to ZZ$, $q\bar{q}' \to WZ$ with $W \to \ell\nu$ and an undetected lepton, and the small contribution from tZ production are estimated from simulation. A third CR of trilepton events, consisting mostly of $q\bar{q}' \to WZ$ events, is used to constrain the $q\bar{q}' \to WZ$ background and, most importantly, the large $q\bar{q} \to ZZ$ background. The ability to constrain $q\bar{q} \to ZZ$ from $q\bar{q}' \to WZ$ is based on the similarity in the physics of these processes.

Further details on event selection, kinematic observables, and the methods to estimate the different contributions are discussed in the Methods section.

$2\ell 2\nu$ kinematic observables

The analysis of off-shell H boson events is based on m_{ZZ}. This quantity is computed from the reconstructed momenta in the 4ℓ final state as the invariant mass of the 4ℓ system, $m_{4\ell}$. However, because of the undetected neutrinos, we can only use the transverse mass m_T^{ZZ}, defined below, as a proxy for m_{ZZ} in the $2\ell 2\nu$ final state. First, we identify $\vec{p}_T^{\,\mathrm{miss}}$ as the transverse momentum vector of the Z boson decaying into neutrinos. Since there is no information on the longitudinal momenta of the neutrinos, m_T^{ZZ} is then computed as the invariant mass of the ZZ pair with all longitudinal momenta set to zero. This results in a variable with a distribution that peaks at m_{ZZ}, with a long tail towards lower values. The definition of m_T^{ZZ} is

$$\left(m_T^{ZZ}\right)^2 = \left[\sqrt{p_T^{\ell\ell\,2} + m_{\ell\ell}{}^2} + \sqrt{p_T^{\mathrm{miss}\,2} + m_Z{}^2}\right]^2 - \left|\vec{p}_T^{\,\ell\ell} + \vec{p}_T^{\,\mathrm{miss}}\right|^2,$$

where $\vec{p}_T^{\,\ell\ell}$ and $m_{\ell\ell}$ are the dilepton transverse momentum and invariant mass, respectively, and m_Z, the Z boson pole mass, is taken to be $91.2\,\mathrm{GeV}$.

The kinematic quantity p_T^{miss} itself is used as another observable to discriminate processes with genuine, large p_T^{miss} against the Z+jets background. Finally, in events with at least two jets, we use matrix element (MELA [26]) kinematic discriminants that distinguish the VBF process from the gg process or SM backgrounds. These discriminants are the $\mathcal{D}_{2\mathrm{jet}}^{\mathrm{VBF}}$-type kinematic discriminants used in Refs. [15, 23], and are based on the four-momenta of the H boson and the two jets leading in p_T.

Data interpretation

The results for the off-shell signal strength parameters $\mu_F^{\mathrm{off\text{-}shell}}$, $\mu_V^{\mathrm{off\text{-}shell}}$, and $\mu^{\mathrm{off\text{-}shell}}$, and the H boson width Γ_H are extracted from binned extended maximum likelihood fits over several kinematic distributions following the parametrization in Ref. [15]. In this parametrization, all mass dependencies are absorbed into the distributions for the various terms contributing to the likelihood, and the off-shell signal strength parameters, or Γ_H, are kept mass-independent. Over different data periods and event categories, 117 multidimensional distributions are used in the fit: 42 for off-shell $2\ell 2\nu$ data (10 867 events), including 18 distributions from the trilepton WZ CR (8541 events), and 18 and 57 for off-shell and on-shell 4ℓ data (1407 off-shell and 621 on-shell events), respectively.

In the $2\ell 2\nu$ data sample, the value of m_T^{ZZ} is required to be greater than $300\,\mathrm{GeV}$. Depending on the number of jets (N_j), this sample is binned in m_T^{ZZ} and p_T^{miss} ($N_j < 2$), or m_T^{ZZ}, p_T^{miss}, and the $\mathcal{D}_{2\mathrm{jet}}^{\mathrm{VBF}}$-type kinematic discriminants ($N_j \geq 2$). For the 4ℓ samples, the binning is in $m_{4\ell}$ and MELA discriminants, which are sensitive to differences between the H boson signal and continuum ZZ production, or the interfering amplitudes, or anomalous HVV couplings. These variables are listed in Table II of Ref. [15] for 4ℓ off-shell data, under 'Scheme 2' in Table IV of Ref. [23] for on-shell 2016-2018 data, and in Table 1 of Ref. [15] for on-shell 2015 data. The $m_{4\ell}$ range is required to be within 105–$140\,\mathrm{GeV}$ for 4ℓ on-shell data, or above $220\,\mathrm{GeV}$ for 4ℓ off-shell data.

Theoretical uncertainties in the kinematic distributions include the simulation of extra jets (up to 20% depending on N_j), and the quantum chromodynamic (QCD) running scale and parton distribution function (PDF) uncertainties in the cross section calculation (up to 30% and 20%, respectively, depending on the process, and m_T^{ZZ} or $m_{4\ell}$). These are particularly important in the gg process since it cannot be constrained by the trilepton WZ CR. Theory uncertainties also

include those associated with the EW corrections to the $q\overline{q} \to ZZ$ and WZ processes, which reach 20% at masses around 1 TeV [31, 32].

Experimental uncertainties include uncertainties in the lepton reconstruction and trigger efficiency (typically 1% per lepton), the integrated luminosity (between 1.2% and 2.5%, depending on the data-taking period [33–35]), and the jet energy scale and resolution [36], which affect the counting of jets, as well as the reconstruction of the VBF discriminants.

Evidence for off-shell contributions, and width measurement

A representative distribution of m_T^{ZZ}, integrated over all N_j, is shown for $2\ell2\nu$ events on the left panel of Fig. 3. Finer details in terms of N_j and the various contributions to the event sample are displayed in Extended Data Fig. 4. The CRs for instrumental $p_\mathrm{T}^\mathrm{miss}$ and nonresonant dilepton production backgrounds are illustrated in Extended Data Figs. 5 and 6, respectively, and the CR with trilepton WZ events is illustrated in Extended Data Fig. 7. Also shown on the right panel of Fig. 3 is a representative distribution of $m_{4\ell}$ from the combined off-shell 4ℓ events.
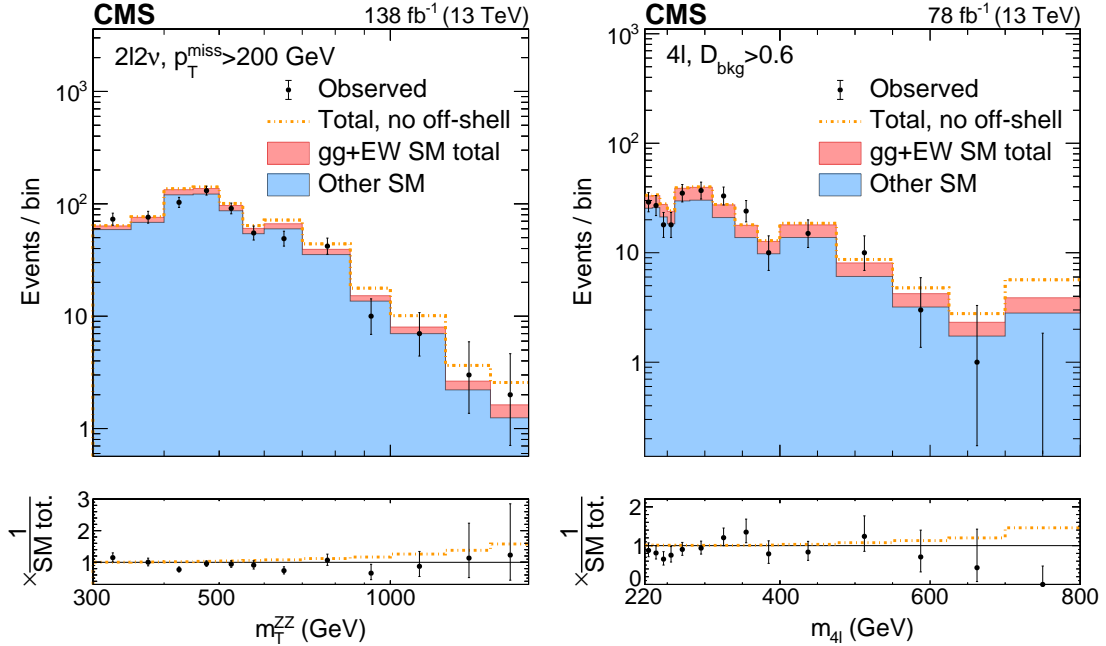
Figure 3: **Distributions of ZZ invariant mass observables in the off-shell signal regions.** The distributions of transverse ZZ invariant mass, m_T^{ZZ} from the $2\ell2\nu$ off-shell signal region are displayed on the left panel, and those of the 4ℓ invariant mass, $m_{4\ell}$, from the 4ℓ off-shell signal region are displayed on the right. The stacked histogram displays the distribution after a fit to the data with SM couplings, with the blue filled area corresponding to the SM processes that do not include H boson interactions, and the pink filled area adding processes that include H boson and interference contributions. The gold dot-dashed line shows the fit to the no off-shell hypothesis. The black points with error bars as uncertainties at 68% CL show the observed data, which is consistent with the prediction with SM couplings within one standard deviation. The last bins contain the overflow. The requirements on the missing transverse momentum $p_\mathrm{T}^\mathrm{miss}$ in $2\ell2\nu$ events, and the $\mathcal{D}_\mathrm{bkg}$-type kinematic background discriminants (see Table II of Ref. [15]) in 4ℓ events are applied in order to enhance the H boson signal contribution. The values of integrated luminosity displayed correspond to those included in the off-shell analyses of each final state. The bottom panels show the ratio of the data or dashed histograms to the SM prediction (stacked histogram). The black horizontal line in these panels marks unit ratio.

The constraints on $\mu_F^{\text{off-shell}}$, $\mu_V^{\text{off-shell}}$, $\mu^{\text{off-shell}}$, and Γ_H are summarized in Table 1, where we show the "observed" results, i.e., those extracted from data, as well as the "expected" ones, i.e., those based on the SM and our understanding of selection efficiencies, backgrounds, and systematic uncertainties. The two set of results are consistent with statistical fluctuations in the data. The constraint on Γ_H at 95% confidence level corresponds to $7.7 \times 10^{-23} < \tau_H < 1.3 \times 10^{-21}$ s in H boson lifetime.

The profile likelihood scans in the $\mu_F^{\text{off-shell}}$ and $\mu_V^{\text{off-shell}}$ plane are shown on the left panel of Fig. 4; scans over the individual signal strengths are in Extended Data Fig. 8. Likelihood scans over Γ_H are displayed in the right panel of Fig. 4. These scans always include information from the 4ℓ on-shell data, and the three cases displayed correspond to adding the 4ℓ off-shell data alone, the $2\ell2\nu$ off-shell data alone, or adding both. The steepness of the slope of the log-likelihood curves near $\mu^{\text{off-shell}} = 0$ and $\Gamma_H = 0$ MeV is caused by the interference terms between the H boson and continuum ZZ production amplitudes that scale with $\sqrt{\mu^{\text{off-shell}}}$ or $\sqrt{\Gamma_H}$, respectively.

The no off-shell scenario with $\mu^{\text{off-shell}} = 0$, or $\Gamma_H = 0$ MeV is excluded at a p-value of 0.0003 (3.6 standard deviations). The p-value calculation is checked with pseudoexperiments and the Feldman-Cousins prescription [37]. As described in greater detail in the Methods section, the exclusion is illustrated in Extended Data Fig. 9 through a comparison of the total number of events in each off-shell signal region bin predicted for the fit of the data to the no off-shell scenario, and the best fit. Constraints on Γ_H are stable within 1 MeV (0.1 MeV) for the upper (lower) limits when testing the presence of anomalous HVV couplings. More results on these anomalous couplings are discussed in the Methods section, and can be found in Extended Data Fig. 8 and Extended Data Table 1. All results are also tabulated in the HEPData record for this analysis [38].

Table 1: **Results on the off-shell signal strengths and Γ_H.** The various fit conditions are indicated in the column labeled "Cond.": Results on $\mu^{\text{off-shell}}$ are presented with $R_{V,F}^{\text{off-shell}} = \mu_V^{\text{off-shell}} / \mu_F^{\text{off-shell}}$ either unconstrained (u) or $= 1$, and constraints on $\mu_F^{\text{off-shell}}$ and $\mu_V^{\text{off-shell}}$ are shown with the other signal strength unconstrained. Results on Γ_H (in units of MeV) are obtained with the on-shell signal strengths unconstrained, and the different conditions listed for this quantity reflect which off-shell final states are combined with on-shell 4ℓ data. The expected central values, not quoted explicitly in this table, are either unity for $\mu^{\text{off-shell}}$, $\mu_F^{\text{off-shell}}$, and $\mu_V^{\text{off-shell}}$, or $\Gamma_H = 4.1$ MeV.

Param.	Cond.	Observed		Expected	
		68% CL	95% CL	68% CL	95% CL
$\mu_F^{\text{off-shell}}$	$\mu_V^{\text{off-shell}}$ (u)	$0.62^{+0.68}_{-0.45}$	$^{+1.38}_{-0.614}$	$^{+1.1}_{-0.99998}$	< 3.0
$\mu_V^{\text{off-shell}}$	$\mu_F^{\text{off-shell}}$ (u)	$0.90^{+0.9}_{-0.59}$	$^{+2.0}_{-0.849}$	$^{+2.0}_{-0.89}$	< 4.5
$\mu^{\text{off-shell}}$	$R_{V,F}^{\text{off-shell}} = 1$	$0.74^{+0.56}_{-0.38}$	$^{+1.06}_{-0.61}$	$^{+1.0}_{-0.84}$	$^{+1.7}_{-0.9914}$
	$R_{V,F}^{\text{off-shell}}$ (u)	$0.62^{+0.68}_{-0.45}$	$^{+1.38}_{-0.6139}$	$^{+1.1}_{-0.99996}$	$^{+2.0}_{-0.99999}$
Γ_H	$2\ell2\nu + 4\ell$	$3.2^{+2.4}_{-1.7}$	$^{+5.3}_{-2.7}$	$^{+4.0}_{-3.5}$	$^{+7.2}_{-4.07}$
Γ_H	$2\ell2\nu$	$3.1^{+3.4}_{-2.1}$	$^{+7.3}_{-2.9}$	$^{+5.1}_{-3.7}$	$^{+9.1}_{-4.099}$
Γ_H	4ℓ	$3.8^{+3.8}_{-2.7}$	$^{+8.0}_{-3.73}$	$^{+5.1}_{-4.05}$	< 13.8
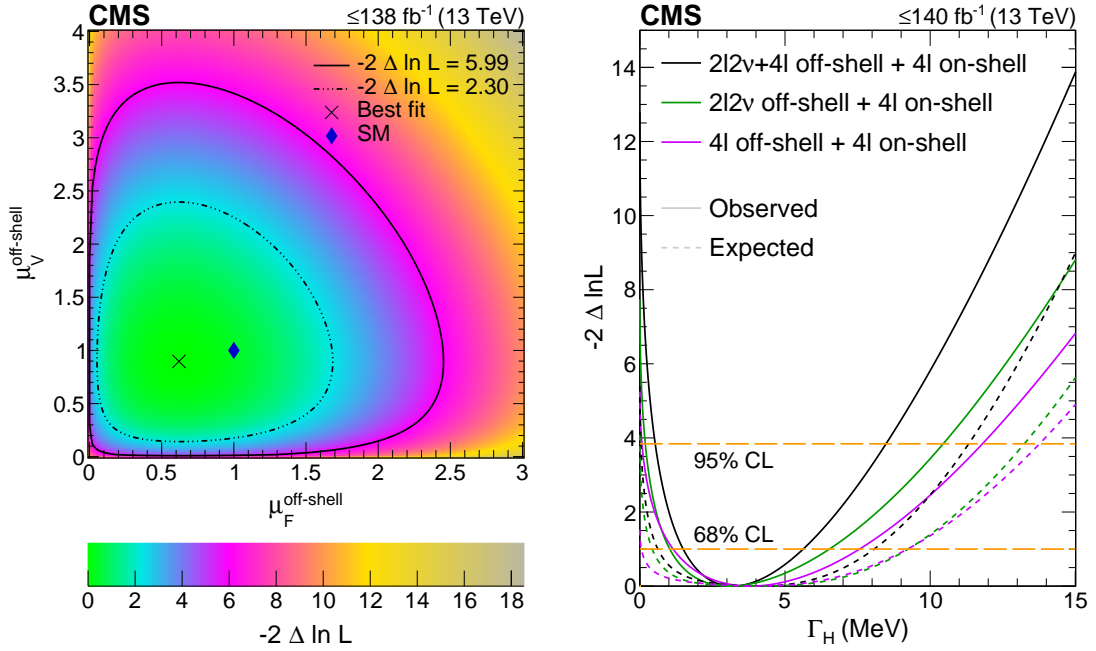
Figure 4: **Log-likelihood scans of $\mu_{\mathrm{F}}^{\mathrm{off\text{-}shell}}$ and $\mu_{\mathrm{V}}^{\mathrm{off\text{-}shell}}$, and Γ_{H}.** Left panel: Two-parameter likelihood scan of the off-shell gg and EW production signal strength parameters, $\mu_{\mathrm{F}}^{\mathrm{off\text{-}shell}}$ and $\mu_{\mathrm{V}}^{\mathrm{off\text{-}shell}}$, respectively. The dot-dashed and dashed contours enclose the 68% ($-2\Delta \ln \mathcal{L} = 2.30$) and 95% ($-2\Delta \ln \mathcal{L} = 5.99$) CL regions. The cross marks the minimum, and the blue diamond marks the SM expectation. The integrated luminosity reaches only up to $138\,\mathrm{fb}^{-1}$ as on-shell 4ℓ events are not included in performing this scan. Right panel: The observed (solid) and expected (dashed) one-parameter likelihood scans over Γ_{H}. Scans are shown for the combination of 4ℓ on-shell data with 4ℓ off-shell (magenta) or $2\ell2\nu$ off-shell data (green) alone, or with both data sets (black). The horizontal lines indicate the 68% ($-2\Delta \ln \mathcal{L} = 1.0$) and 95% ($-2\Delta \ln \mathcal{L} = 3.84$) CL regions. The integrated luminosity reaches up to $140\,\mathrm{fb}^{-1}$ as on-shell 4ℓ events are included in performing these scans. The exclusion of the no off-shell hypothesis is consistent with 3.6 standard deviations on both panels.

References

[1] F. Englert and R. Brout, "Broken symmetry and the mass of gauge vector mesons", *Phys. Rev. Lett.* **13** (1964) 321–323, `doi:10.1103/PhysRevLett.13.321`.

[2] P. W. Higgs, "Broken symmetries and the masses of gauge bosons", *Phys. Rev. Lett.* **13** (1964) 508–509, `doi:10.1103/PhysRevLett.13.508`.

[3] G. S. Guralnik, C. R. Hagen, and T. W. B. Kibble, "Global conservation laws and massless particles", *Phys. Rev. Lett.* **13** (1964) 585–587, `doi:10.1103/PhysRevLett.13.585`.

[4] ATLAS Collaboration, "Observation of a new particle in the search for the Standard Model Higgs boson with the ATLAS detector at the LHC", *Phys. Lett. B* **716** (2012) 1–29, `doi:10.1016/j.physletb.2012.08.020`, `arXiv:1207.7214`.

[5] CMS Collaboration, "Observation of a new boson at a mass of 125 GeV with the CMS experiment at the LHC", *Phys. Lett. B* **716** (2012) 30–61, `doi:10.1016/j.physletb.2012.08.021`, `arXiv:1207.7235`.

[6] CMS Collaboration, "Observation of a new boson with mass near 125 GeV in pp collisions at $\sqrt{s} = 7$ and 8 TeV", *JHEP* **06** (2013) 081, `doi:10.1007/JHEP06(2013)081`, `arXiv:1303.4571`.

[7] W. Heisenberg, "Über den anschaulichen inhalt der quantentheoretischen kinematik und mechanik", *Z. Phys.* **43** (1927) 172–198, `doi:10.1007/BF01397280`.

[8] G. Breit and E. Wigner, "Capture of slow neutrons", *Phys. Rev.* **49** (1936) 519–531, `doi:10.1103/PhysRev.49.519`.

[9] ALEPH, DELPHI, L3, OPAL, SLD, LEP Electroweak Working Group, SLD Electroweak Group, SLD Heavy Flavour Group Collaboration, "Precision electroweak measurements on the Z resonance", *Phys. Rept.* **427** (2006) 257–454, `doi:10.1016/j.physrep.2005.12.006`, `arXiv:hep-ex/0509008`.

[10] LHC Higgs Cross Section Working Group, "Handbook of LHC Higgs cross sections: 4. Deciphering the nature of the Higgs sector", CERN Report CERN-2017-002-M, 2016. `doi:10.23731/CYRM-2017-002`, `arXiv:1610.07922`.

[11] CMS Collaboration, "Limits on the Higgs boson lifetime and width from its decay to four charged leptons", *Phys. Rev. D* **92** (2015) 072010, `doi:10.1103/PhysRevD.92.072010`, `arXiv:1507.06656`.

[12] F. Caola and K. Melnikov, "Constraining the Higgs boson width with ZZ production at the LHC", *Phys. Rev. D* **88** (2013) 054024, `doi:10.1103/PhysRevD.88.054024`, `arXiv:1307.4935`.

[13] J. M. Campbell, R. K. Ellis, and C. Williams, "Bounding the Higgs width at the LHC using full analytic results for gg $\to$ e$^-$e$^+\mu^-\mu^+$", *JHEP* **04** (2014) 060, `doi:10.1007/JHEP04(2014)060`, `arXiv:1311.3589`.

[14] ATLAS Collaboration, "Constraints on off-shell Higgs boson production and the Higgs boson total width in ZZ $\to$ 4ℓ and ZZ $\to$ 2ℓ2ν final states with the ATLAS detector", *Phys. Lett. B* **786** (2018) 223–244, `doi:10.1016/j.physletb.2018.09.048`, `arXiv:1808.01191`.

[15] CMS Collaboration, "Measurements of the Higgs boson width and anomalous HVV couplings from on-shell and off-shell production in the four-lepton final state", *Phys. Rev. D* **99** (2019) 112003, `doi:10.1103/PhysRevD.99.112003`, `arXiv:1901.00174`.

[16] C. H. Llewellyn Smith, "High-energy behavior and gauge symmetry", *Phys. Lett. B* **46** (1973) 233–236, `doi:10.1016/0370-2693(73)90692-8`.

[17] J. M. Cornwall, D. N. Levin, and G. Tiktopoulos, "Derivation of gauge invariance from high-energy unitarity bounds on the *S*-matrix", *Phys. Rev. D* **10** (1974) 1145–1167, `doi:10.1103/PhysRevD.10.1145`. Erratum, `doi:10.1103/PhysRevD.11.972`.

[18] B. W. Lee, C. Quigg, and H. B. Thacker, "Weak interactions at very high-energies: the role of the Higgs boson mass", *Phys. Rev. D* **16** (1977) 1519–1531, `doi:10.1103/PhysRevD.16.1519`.

[19] E. W. N. Glover and J. J. van der Bij, "Z boson pair production via gluon fusion", *Nucl. Phys. B* **321** (1989) 561–590, `doi:10.1016/0550-3213(89)90262-9`.

[20] F. Campanario, Q. Li, M. Rauch, and M. Spira, "ZZ+jet production via gluon fusion at the LHC", *JHEP* **06** (2013) 069, `doi:10.1007/JHEP06(2013)069`, `arXiv:1211.5429`.

[21] N. Kauer and G. Passarino, "Inadequacy of zero-width approximation for a light Higgs boson signal", *JHEP* **08** (2012) 116, `doi:10.1007/JHEP08(2012)116`, `arXiv:1206.4803`.

[22] CMS Collaboration, "Constraints on anomalous Higgs boson couplings using production and decay information in the four-lepton final state", *Phys. Lett. B* **775** (2017) 1–24, `doi:10.1016/j.physletb.2017.10.021`, `arXiv:1707.00541`.

[23] CMS Collaboration, "Constraints on anomalous Higgs boson couplings to vector bosons and fermions in its production and decay using the four-lepton final state", *Phys. Rev. D* **104** (2021) 052004, `doi:10.1103/PhysRevD.104.052004`, `arXiv:2104.12152`.

[24] J. S. Gainer et al., "Beyond geolocating: Constraining higher dimensional operators in $H \to 4\ell$ with off-shell production and more", *Phys. Rev. D* **91** (2015) 035011, `doi:10.1103/PhysRevD.91.035011`, `arXiv:1403.4951`.

[25] C. Englert and M. Spannowsky, "Limitations and opportunities of off-shell coupling measurements", *Phys. Rev. D* **90** (2014) 053003, `doi:10.1103/PhysRevD.90.053003`, `arXiv:1405.0285`.

[26] A. V. Gritsan et al., "New features in the JHU generator framework: constraining Higgs boson properties from on-shell and off-shell production", *Phys. Rev. D* **102** (2020) 056022, `doi:10.1103/PhysRevD.102.056022`, `arXiv:2002.09888`.

[27] U. Sarica, "Measurements of Higgs boson properties in proton-proton collisions at $\sqrt{s} = 7, 8$ and 13 TeV at the CERN Large Hadron Collider". PhD thesis, Johns Hopkins U., 2019. `doi:10.1007/978-3-030-25474-2`.

[28] CMS Collaboration, "Measurements of $t\bar{t}H$ production and the CP structure of the Yukawa interaction between the Higgs boson and top quark in the diphoton decay channel", *Phys. Rev. Lett.* **125** (2020) 061801, `doi:10.1103/PhysRevLett.125.061801`, `arXiv:2003.10866`.

[29] ATLAS Collaboration, "CP properties of Higgs boson interactions with top quarks in the $t\bar{t}H$ and tH processes using $H \to \gamma\gamma$ with the ATLAS detector", *Phys. Rev. Lett.* **125** (2020) 061802, `doi:10.1103/PhysRevLett.125.061802`, `arXiv:2004.04545`.

[30] SMEFiT Collaboration, "Combined SMEFT interpretation of Higgs, diboson, and top quark data from the LHC", *JHEP* **11** (2021) 089, `doi:10.1007/JHEP11(2021)089`, `arXiv:2105.00006`.

[31] A. Bierweiler, T. Kasprzik, and J. H. Kühn, "Vector-boson pair production at the LHC to $\mathcal{O}(\alpha^3)$ accuracy", *JHEP* **12** (2013) 071, `doi:10.1007/JHEP12(2013)071`, `arXiv:1305.5402`.

[32] A. Manohar, P. Nason, G. P. Salam, and G. Zanderighi, "How bright is the proton? A precise determination of the photon parton distribution function", *Phys. Rev. Lett.* **117** (2016) 242002, `doi:10.1103/PhysRevLett.117.242002`, `arXiv:1607.04266`.

[33] CMS Collaboration, "Precision luminosity measurement in proton-proton collisions at $\sqrt{s} = 13$ TeV in 2015 and 2016 at CMS", *Eur. Phys. J. C* **81** (2021) 800, `doi:10.1140/epjc/s10052-021-09538-2`, `arXiv:2104.01927`.

[34] CMS Collaboration, "CMS luminosity measurement for the 2017 data-taking period at $\sqrt{s} = 13$ TeV", CMS Physics Analysis Summary CMS-PAS-LUM-17-004, 2018.

[35] CMS Collaboration, "CMS luminosity measurement for the 2018 data-taking period at $\sqrt{s} = 13$ TeV", CMS Physics Analysis Summary CMS-PAS-LUM-18-002, 2019.

[36] CMS Collaboration, "Jet energy scale and resolution in the CMS experiment in pp collisions at 8 TeV", *JINST* **12** (2017) P02014, `doi:10.1088/1748-0221/12/02/P02014`, `arXiv:1607.03663`.

[37] G. J. Feldman and R. D. Cousins, "A unified approach to the classical statistical analysis of small signals", *Phys. Rev. D* **57** (1998) 3873–3889, `doi:10.1103/PhysRevD.57.3873`, `arXiv:physics/9711021`.

[38] CMS Collaboration. HEPData record for this analysis, 2022. `doi:10.17182/hepdata.127288`.

[39] CMS Collaboration, "The CMS experiment at the CERN LHC", *JINST* **3** (2008) S08004, `doi:10.1088/1748-0221/3/08/S08004`.

[40] CMS Collaboration, "The CMS trigger system", *JINST* **12** (2017) P01020, `doi:10.1088/1748-0221/12/01/P01020`, `arXiv:1609.02366`.

[41] CMS Collaboration, "Performance of the CMS muon detector and muon reconstruction with proton-proton collisions at $\sqrt{s} = 13$ TeV", *JINST* **13** (2018) P06015, `doi:10.1088/1748-0221/13/06/P06015`, `arXiv:1804.04528`.

[42] CMS Collaboration, "Electron and photon reconstruction and identification with the CMS experiment at the CERN LHC", *JINST* **16** (2021) P05014, `doi:10.1088/1748-0221/16/05/P05014`, `arXiv:2012.06888`.

[43] CMS Collaboration, "Description and performance of track and primary-vertex reconstruction with the CMS tracker", *JINST* **9** (2014) P10009, `doi:10.1088/1748-0221/9/10/P10009`, `arXiv:1405.6569`.

[44] CMS Collaboration, "Particle-flow reconstruction and global event description with the CMS detector", *JINST* **12** (2017) P10003, `doi:10.1088/1748-0221/12/10/P10003`, `arXiv:1706.04965`.

[45] CMS Collaboration, "Performance of missing transverse momentum reconstruction in proton-proton collisions at $\sqrt{s} = 13\,\text{TeV}$ using the CMS detector", *JINST* **14** (2019) P07004, `doi:10.1088/1748-0221/14/07/P07004`, `arXiv:1903.06078`.

[46] CMS Collaboration, "Performance of reconstruction and identification of τ leptons decaying to hadrons and ν_τ in pp collisions at $\sqrt{s} = 13\,\text{TeV}$", *JINST* **13** (2018) P10005, `doi:10.1088/1748-0221/13/10/P10005`, `arXiv:1809.02816`.

[47] CMS Collaboration, "Measurements of inclusive W and Z cross sections in pp collisions at $\sqrt{s} = 7\,\text{TeV}$", *JHEP* **01** (2011) 080, `doi:10.1007/JHEP01(2011)080`, `arXiv:1012.2466`.

[48] M. Cacciari, G. P. Salam, and G. Soyez, "FastJet user manual", *Eur. Phys. J. C* **72** (2012) 1896, `doi:10.1140/epjc/s10052-012-1896-2`, `arXiv:1111.6097`.

[49] CMS Collaboration, "Pileup mitigation at CMS in 13 TeV data", *JINST* **15** (2020) P09018, `doi:10.1088/1748-0221/15/09/P09018`, `arXiv:2003.00503`.

[50] E. Bols et al., "Jet flavour classification using DeepJet", *JINST* **15** (2020) 12012, `doi:10.1088/1748-0221/15/12/P12012`, `arXiv:2008.10519`.

[51] CMS Collaboration, "Missing transverse energy performance of the CMS detector", *JINST* **6** (2011) P09001, `doi:10.1088/1748-0221/6/09/P09001`, `arXiv:1106.5048`.

[52] S. Frixione, P. Nason, and C. Oleari, "Matching NLO QCD computations with parton shower simulations: the POWHEG method", *JHEP* **11** (2007) 070, `doi:10.1088/1126-6708/2007/11/070`, `arXiv:0709.2092`.

[53] P. Nason and C. Oleari, "NLO Higgs boson production via vector-boson fusion matched with shower in POWHEG", *JHEP* **02** (2010) 037, `doi:10.1007/JHEP02(2010)037`, `arXiv:0911.5299`.

[54] E. Bagnaschi, G. Degrassi, P. Slavich, and A. Vicini, "Higgs production via gluon fusion in the POWHEG approach in the SM and in the MSSM", *JHEP* **02** (2012) 088, `doi:10.1007/JHEP02(2012)088`, `arXiv:1111.2854`.

[55] G. Luisoni, P. Nason, C. Oleari, and F. Tramontano, "HW$^\pm$/HZ + 0 and 1 jet at NLO with the POWHEG BOX interfaced to GoSam and their merging within MiNLO", *JHEP* **10** (2013) 083, `doi:10.1007/JHEP10(2013)083`, `arXiv:1306.2542`.

[56] J. M. Campbell and R. K. Ellis, "MCFM for the Tevatron and the LHC", *Nucl. Phys. Proc. Suppl.* **205–206** (2010) 10–15, `doi:10.1016/j.nuclphysbps.2010.08.011`, `arXiv:1007.3492`.

[57] J. M. Campbell, R. K. Ellis, and C. Williams, "Vector boson pair production at the LHC", *JHEP* **07** (2011) 018, `doi:10.1007/JHEP07(2011)018`, `arXiv:1105.0020`.

[58] J. M. Campbell and R. K. Ellis, "Higgs constraints from vector boson fusion and scattering", *JHEP* **04** (2015) 030, `doi:10.1007/JHEP04(2015)030`, `arXiv:1502.02990`.

[59] Particle Data Group, P. A. Zyla et al., "Review of Particle Physics", *PTEP* **2020** (2020) 083C01, `doi:10.1093/ptep/ptaa104`.

[60] M. Grazzini, S. Kallweit, and M. Wiesemann, "Fully differential NNLO computations with MATRIX", *Eur. Phys. J. C* **78** (2018) 537, `doi:10.1140/epjc/s10052-018-5771-7`, `arXiv:1711.06631`.

[61] R. Frederix and S. Frixione, "Merging meets matching in MC@NLO", *JHEP* **12** (2012) 061, `doi:10.1007/JHEP12(2012)061`, `arXiv:1209.6215`.

[62] J. Alwall et al., "Comparative study of various algorithms for the merging of parton showers and matrix elements in hadronic collisions", *Eur. Phys. J. C* **53** (2008) 473–500, `doi:10.1140/epjc/s10052-007-0490-5`, `arXiv:0706.2569`.

[63] T. Sjöstrand et al., "An introduction to PYTHIA 8.2", *Comput. Phys. Commun.* **191** (2015) 159–177, `doi:10.1016/j.cpc.2015.01.024`, `arXiv:1410.3012`.

[64] CMS Collaboration, "Event generator tunes obtained from underlying event and multiparton scattering measurements", *Eur. Phys. J. C* **76** (2016) 155, `doi:10.1140/epjc/s10052-016-3988-x`, `arXiv:1512.00815`.

[65] CMS Collaboration, "Extraction and validation of a new set of CMS PYTHIA8 tunes from underlying-event measurements", *Eur. Phys. J. C* **80** (2020) 4, `doi:10.1140/epjc/s10052-019-7499-4`, `arXiv:1903.12179`.

[66] NNPDF Collaboration, "Parton distributions for the LHC Run II", *JHEP* **04** (2015) 040, `doi:10.1007/JHEP04(2015)040`, `arXiv:1410.8849`.

[67] GEANT4 Collaboration, "GEANT4—a simulation toolkit", *Nucl. Instrum. Meth. A* **506** (2003) 250–303, `doi:10.1016/S0168-9002(03)01368-8`.

[68] CMS Collaboration, "Search for physics beyond the standard model in events with a Z boson, jets, and missing transverse energy in pp collisions at $\sqrt{s} = 7$ TeV", *Phys. Lett. B* **716** (2012) 260–284, `doi:10.1016/j.physletb.2012.08.026`, `arXiv:1204.3774`.

Methods

Experimental setup

The CMS apparatus [39] is a multipurpose, nearly hermetic detector, designed to trigger on [40] and identify muons, electrons, photons, and charged or neutral hadrons [41–43]. A global reconstruction algorithm, particle-flow (PF) [44], combines the information provided by the all-silicon inner tracker and by the crystal electromagnetic and brass-scintillator hadron calorimeters (ECAL and HCAL, respectively), operating inside a 3.8 T superconducting solenoid, with data from gas-ionization muon detectors interleaved with the solenoid return yoke, to build jets, missing transverse momentum, tau leptons, and other physics objects [36, 45, 46]. In the following discussion up to likelihood scans, we will focus on the details of the $2\ell2\nu$ analysis. Analysis details for the off-shell 4ℓ data can be found in Ref. [15], 2015 on-shell 4ℓ data in Refs. [15, 22], and 2016–2018 on-shell 4ℓ data in Ref. [23].

Physics objects

Events in the $2\ell2\nu$ signal region, the $e\mu$ CR, and the trilepton WZ CR are selected using single-lepton and dilepton triggers. The efficiencies of these selections are measured using orthogonal triggers, i.e., jet or p_T^{miss} triggers, and events triggered on a third, isolated lepton, or a jet. They range between 78% and 100%, depending on the flavor of the leptons, and p_T and η of the dilepton system, taking lower values at lower p_T. Photon triggers are used to collect events for the γ+jets CR. The photon trigger efficiency is measured using a tag-and-probe method [47] in $Z \to ee$ events, with one electron interpreted as a photon with tracks ignored, as well as through a study of $\ell\ell\gamma$ events. The efficiency is found to range from $\sim$55% at 55 GeV in photon p_T to $\sim$95% at photon $p_T > 220$ GeV.

Jets are reconstructed using the anti-k_T algorithm [48] with a distance parameter of 0.4. Jet energies are corrected for instrumental effects, as well as for the contribution of particles originating from additional pp interactions (pileup). A multivariate technique is used to suppress jets from pileup interactions [49]. For the purpose of this analysis, we select jets of $p_T > 30$ GeV and $|\eta| < 4.7$, and they must be separated by $\Delta R = \sqrt{(\Delta\phi)^2 + (\Delta\eta)^2} > 0.4$, with ϕ being the azimuthal angle measured in radians, from a lepton or a photon of interest. Jets within $|\eta| < 2.5$ ($|\eta| < 2.4$ for 2016 data) can be identified as b jets using the DEEPJET algorithm [50] with a loose working point. The efficiency of this working point ranges between 75% and 95%, depending on p_T, η, and the data period.

The missing transverse momentum vector $\vec{p}_T^{miss}$ is estimated from the negative of the vector sum of the transverse momenta of all PF candidates. Dedicated algorithms [51] are used to eliminate events featuring cosmic ray contributions, beam-gas interactions, beam halo, or calorimetric noise.

The algorithms to reconstruct leptons are described in detail in Ref. [41] for muons and Ref. [42] for electrons. Muons are identified using a set of requirements on individual variables, while electrons are identified using a boosted decision tree algorithm. Leptons of interest in this analysis are expected to be isolated with respect to the activity in the rest of the event. A measure of isolation is computed from the flux of photons and hadrons reconstructed by the PF algorithm that are within a cone of $\Delta R < 0.3$ built around the lepton direction, including corrections from the contributions of pileup. We define loose and tight isolation requirements for muons (electrons) with $p_T > 5$ GeV and $|\eta| < 2.4$ ($|\eta| < 2.5$). The efficiency of loose selection for muons (electrons) ranges from $\sim$85% (65–75%, depending on η) at $p_T = 5$ GeV to $> 90\%$ ($> 85\%$) at $p_T > 25$ GeV. The additional requirements for tight selections reduce efficiencies by

10–15%.

Photons are reconstructed from energy clusters in the ECAL not linked to charged tracks, with the exception of converted photons [42]. Their energies are corrected for shower containment in the ECAL crystals and energy loss due to conversions in the tracker with a multivariate regression. In this analysis, we consider photons with $p_T > 20\,\text{GeV}$ and $|\eta|$ up to 2.5, with requirements on shower shape and isolation used to identify isolated photons and separate them from hadronic jets. The selection requirements are tightened in the γ+jets CR, which leads to selection efficiencies in the range 50–75%, depending on p_T and η.

Event simulation

The signal Monte Carlo (MC) samples are generated for an undecayed H boson for gg, VBF, ZH, and WH productions using the POWHEG 2 [52–55] program at next-to-leading order (NLO) in QCD at various H boson pole masses, ranging from 125 GeV to 3 TeV. The generated H bosons are decayed to four-fermion final states through intermediate Z bosons using the JHUGEN [26] program, with versions between 6.9.8 and 7.4.0.

These samples are reweighted using the MELA matrix element package, which interfaces with the JHUGEN and MCFM [13, 56–58] matrix elements, following the same reweighting techniques used in Ref. [15] to obtain the final ZZ event sample, including the H boson contribution, the continuum, and their interference. The MELAANALYTICS package developed for Ref. [15] is used to automate matrix element computations and to account for the extra partons in the NLO simulation. The gg generation is rescaled with the next-to-NLO (NNLO) QCD K-factor, differential in m_{VV}, and an additional uniform K-factor of 1.10 for the next-to-NNLO cross section computed at $m_H = 125\,\text{GeV}$ [10]. Furthermore, the pole mass values of the top quark (173 GeV) and the bottom quark (4.8 GeV) [59] are used in the massive loop calculations for the generation of this process. The difference that would be introduced by using the $\overline{\text{MS}}$ renormalization scheme for these masses is found to be within the systematic uncertainties after accounting for the effects on both the H boson and continuum ZZ amplitudes.

The tree-level Feynman diagrams in Fig. 1 illustrate the complete set contributing to the gg $\rightarrow$ ZZ process on the leftmost top and bottom panels, and some of the diagrams contributing to the EW ZZ production associated with two fermions on the middle and top right panels. Extended Data Figs. 1 and 2 display the full set of diagrams for the EW process.

The q$\overline{\text{q}}$ $\rightarrow$ ZZ and WZ MC samples are also generated with POWHEG 2 applying EW NLO corrections for two on-shell Z and W bosons [31, 32], and NNLO QCD corrections as a function of m_{VV} [60]. The tree-level Feynman diagrams for these noninterfering continuum contributions are illustrated in Extended Data Fig. 3. Samples for the tZ+X processes, or other processes contributing to the CRs, are generated using MADGRAPH5_aMC@NLO at NLO or LO precision using the FxFx [61] or MLM [62] schemes, respectively, to match jets from matrix element calculations and parton shower.

The parton shower and hadronization are modeled with PYTHIA (8.205 or 8.230) [63], using tunes CUETP8M1 [64] for the 2015 and 2016 data sets, and CP5 [65] for the 2017 and 2018 periods. The PDFs are taken from NNPDF 3.0 [66] with QCD orders matching those of the cross section calculations. Finally, the detector response is simulated with the GEANT4 [67] package.

Signal region selection requirements

Events in the $2\ell 2\nu$ final state are required to have two opposite-sign, same-flavor leptons ($\mu^+\mu^-$ or e^+e^-) satisfying tight isolation requirements with $p_T > 25\,\text{GeV}$, $m_{\ell\ell}$ within $15\,\text{GeV}$ of m_Z, and $p_T^{\ell\ell} > 55\,\text{GeV}$. Additional requirements are imposed to reduce contributions from Z+jets and $t\bar{t}$ processes as follows. Events with b-tagged jets, additional loosely isolated leptons of $p_T > 5\,\text{GeV}$, or additional loosely identified photons with $p_T > 20\,\text{GeV}$ are vetoed. To further improve the effectiveness of the lepton veto, events with isolated reconstructed tracks of $p_T > 10\,\text{GeV}$ are removed. This requirement is also effective against one-prong τ decays.

The value of p_T^{miss} is required to be $> 125\,\text{GeV}$ ($> 140\,\text{GeV}$) for $N_j < 2$ (≥ 2). Requirements are imposed on the unsigned azimuthal opening angles ($\Delta\phi$) between $\vec{p}_T^{\text{miss}}$ and other objects in the event in order to reduce contamination from p_T^{miss} misreconstruction: $\Delta\phi_{\text{miss}}^{\ell\ell} > 1.0$ between $\vec{p}_T^{\text{miss}}$ and $\vec{p}_T^{\ell\ell}$, $\Delta\phi_{\text{miss}}^{\ell\ell+\text{jets}} > 2.5$ between $\vec{p}_T^{\text{miss}}$ and $\vec{p}_T^{\ell\ell} + \sum \vec{p}_T^{j}$, $\min \Delta\phi_{\text{miss}}^{j} > 0.25$ (0.50) between $\vec{p}_T^{\text{miss}}$ and $\vec{p}_T^{j}$ for $N_j = 1$ ($N_j \geq 2$), where $\vec{p}_T^{j}$ is the transverse momentum vector of a jet.

Finally, events are split into lepton flavor ($\mu\mu$ or ee) and jet multiplicity ($N_j = 0, 1, \geq 2$) categories. The resulting event distributions are illustrated along the m_T^{ZZ} observable in Extended Data Fig. 4.

Matrix element kinematic discriminants

In events with $N_j \geq 2$, we use two MELA kinematic discriminants for the VBF process, $\mathcal{D}_{2\text{jet}}^{\text{VBF}}$ and $\mathcal{D}_{2\text{jet}}^{\text{VBF},a2}$ [15]. Each of these discriminants consists of a ratio of two matrix elements, or equivalently a ratio of event-by-event probability functions, expressed in terms of the four-momenta of the H boson and the two jets leading in p_T. The four-momentum of the H boson in the $2\ell 2\nu$ channel is approximated by taking the η of the $Z \to 2\nu$ candidate, together with its sign, to be the same as that of the $Z \to 2\ell$ candidate. This approximation is found to be adequate through MC studies.

In both discriminants, one of matrix elements is always computed for the SM H boson production through gluon fusion. The remaining matrix element is computed for the SM VBF process in $\mathcal{D}_{2\text{jet}}^{\text{VBF}}$, so this discriminant improves the sensitivity to the EW H boson production. The $\mathcal{D}_{2\text{jet}}^{\text{VBF},a2}$ discriminant also computes the remaining matrix element for the VBF process, but under the a_2 HVV coupling hypothesis instead of the SM scenario. We find that this second discriminant brings additional sensitivity to SM backgrounds as well as being sensitive to the a_2 HVV coupling hypothesis by design. When anomalous HVV contributions are considered, the a_2 hypothesis used in the computation is replaced by the appropriate a_i hypothesis to optimize sensitivity for the coupling of interest.

Control regions

As already mentioned, Z+jets events are a background to the $2\ell 2\nu$ signal selection. This can occur because of resolution effects in p_T^{miss} and the large cross section for this process. Since γ+jets and Z+jets have similar production and p_T^{miss} resolution properties, the Z+jets contributions at high p_T^{miss} can be estimated from a γ+jets CR [68].

In this CR, all event selection requirements are the same as those on the signal region, except that the photon replaces the $Z \to \ell\ell$ decay. The m_T^{ZZ} kinematic variable is constructed using the photon p_T in place of $p_T^{\ell\ell}$, and m_Z in place of $m_{\ell\ell}$. Only photons in the barrel region (i.e., $|\eta| < 1.44$) are considered for $N_j < 2$ to eliminate beam halo events that can mimic the

$\gamma + p_\mathrm{T}^\mathrm{miss}$ signature. Reweighting factors are extracted as a function of photon p_T, photon η (when $N_\mathrm{j} \geq 2$), and the number of observed pp collisions by matching the corresponding distributions in γ+jets sidebands at low $p_\mathrm{T}^\mathrm{miss}$ ($< 125\,\mathrm{GeV}$) to those of Z+jets sidebands with the same requirement at each N_j category separately. These reweighting factors are then applied to the high-$p_\mathrm{T}^\mathrm{miss}$ γ+jets data sample. This technique to estimate the background from the data is verified using closure tests from the simulation by comparing the Z+jets and reweighted γ+jets MC distributions over each kinematic observable.

Contributions to the γ+jets CR from events with genuine, large $p_\mathrm{T}^\mathrm{miss}$ from the $\mathrm{Z}(\to \nu\nu)\gamma$, $\mathrm{W}(\to \ell\nu)\gamma$, and $\mathrm{W}(\to \ell\nu)$+jets processes are subtracted in the final estimate of the instrumental $p_\mathrm{T}^\mathrm{miss}$ background. The first two are estimated from simulation, where the $\mathrm{Z}\gamma$ contribution is corrected based on the observed rate of $\mathrm{Z}(\to \ell\ell)\gamma$. The W+jets contribution is estimated from a single-electron sample selected with requirements similar to those in the γ+jets CR. Representative distributions for this estimate are shown in Extended Data Fig. 5.

Processes such as $\mathrm{pp} \to \mathrm{t}\bar{\mathrm{t}}$ and $\mathrm{pp} \to \mathrm{WW}$, including nonresonant H boson contributions, can produce two leptons and large $p_\mathrm{T}^\mathrm{miss}$ without a resonant $\mathrm{Z} \to \ell\ell$ decay. The kinematic properties of the dilepton system in these processes is the same for any combination of lepton flavors e or μ. These nonresonant ee or $\mu\mu$ background processes are therefore estimated from an eμ CR. This CR is constructed applying the same requirements used in the signal selection except for the flavor of the leptons. Data events are reweighted to account for differences in trigger and reconstruction efficiencies between eμ, and ee or $\mu\mu$ final states. Representative distributions for this estimate are shown in Extended Data Fig. 6.

A third CR selects trilepton $\mathrm{q}\bar{\mathrm{q}} \to \mathrm{WZ}$ events. These events are used to constrain the normalization and kinematic properties of the $\mathrm{q}\bar{\mathrm{q}} \to \mathrm{ZZ}$ and WZ continuum contributions. The $\mathrm{Z} \to \ell\ell$ candidate is identified from the opposite-sign, same-flavor lepton pair with $m_{\ell\ell}$ closest to m_Z, and the value of $m_{\ell\ell}$ for this Z candidate is required to be within $15\,\mathrm{GeV}$ of m_Z. Trigger requirements are only placed on this Z candidate. The remaining lepton is identified as the lepton from the W decay (ℓ_W). The leading-p_T lepton from the Z decay is required to satisfy $p_\mathrm{T} > 30\,\mathrm{GeV}$, and the remaining leptons are required to satisfy $p_\mathrm{T} > 20\,\mathrm{GeV}$.

Similar to the signal region, requirements are imposed on the unsigned $\Delta\phi$ between $\vec{p}_\mathrm{T}^\mathrm{miss}$ and other objects in the event in order to reduce contamination from the Z+jets and $\mathrm{q}\bar{\mathrm{q}} \to \mathrm{Z}\gamma$ processes: $\Delta\phi_\mathrm{miss}^{\ell\ell} > 1.0$ between $\vec{p}_\mathrm{T}^\mathrm{miss}$ and $\vec{p}_\mathrm{T}^{\ell\ell}$ for the Z candidate, $\Delta\phi_\mathrm{miss}^{3\ell+\mathrm{jets}} > 2.5$ between $\vec{p}_\mathrm{T}^\mathrm{miss}$ and $\vec{p}_\mathrm{T}^{3\ell} + \sum \vec{p}_\mathrm{T}^\mathrm{j}$, and $\min \Delta\phi_\mathrm{miss}^\mathrm{j} > 0.25$ between $\vec{p}_\mathrm{T}^\mathrm{miss}$ and $\vec{p}_\mathrm{T}^\mathrm{j}$.

The W boson transverse mass is defined through the vector transverse momentum of ℓ_W, $\vec{p}_\mathrm{T}^{\ell_\mathrm{W}}$, as $m_\mathrm{T}^{\ell_\mathrm{W}} = \sqrt{2(p_\mathrm{T}^{\ell_\mathrm{W}} p_\mathrm{T}^\mathrm{miss} - \vec{p}_\mathrm{T}^{\ell_\mathrm{W}} \cdot \vec{p}_\mathrm{T}^\mathrm{miss})}$, and additional requirements are imposed on $p_\mathrm{T}^\mathrm{miss}$ and $m_\mathrm{T}^{\ell_\mathrm{W}}$ in order to reduce contamination from the Z+jets and $\mathrm{q}\bar{\mathrm{q}} \to \mathrm{Z}\gamma$ processes further: $p_\mathrm{T}^\mathrm{miss} > 20\,\mathrm{GeV}$, $m_\mathrm{T}^{\ell_\mathrm{W}} > 20\,\mathrm{GeV}$ ($10\,\mathrm{GeV}$) for $\ell_\mathrm{W} = \mu$ (e), and $\mathrm{A} \times m_\mathrm{T}^{\ell_\mathrm{W}} + p_\mathrm{T}^\mathrm{miss} > 120\,\mathrm{GeV}$, with $\mathrm{A} = 1.6$ (4/3) for $\ell_\mathrm{W} = \mu$ (e). All other requirements on b-tagged jets, and additional leptons or photons are the same as those for the signal region.

The events are finally split into categories of the flavor of ℓ_W (μ or e) and jet multiplicity ($N_\mathrm{j} = 0, 1, \geq 2$), and binned in m_T^WZ, defined using the W boson mass $m_\mathrm{W} = 80.4\,\mathrm{GeV}$ [59] as

$$\left(m_\mathrm{T}^\mathrm{WZ}\right)^2 = \left[\sqrt{p_\mathrm{T}^{\ell\ell 2} + m_{\ell\ell}^2} + \sqrt{\left|\vec{p}_\mathrm{T}^\mathrm{miss} + \vec{p}_\mathrm{T}^{\ell_\mathrm{W}}\right|^2 + m_\mathrm{W}^2}\right]^2 - \left|\vec{p}_\mathrm{T}^{\ell\ell} + \vec{p}_\mathrm{T}^\mathrm{miss} + \vec{p}_\mathrm{T}^{\ell_\mathrm{W}}\right|^2.$$

Event distributions along m_T^{WZ} from this CR are shown in Extended Data Fig. 7.

Likelihood scans

As mentioned in the discussion of data interpretation, the likelihood is constructed from several multidimensional distributions binned over the different event categories. Profile likelihood scans over $\mu_\mathrm{F}^{\text{off-shell}}$, $\mu_\mathrm{V}^{\text{off-shell}}$, $\mu^{\text{off-shell}}$, and Γ_H are shown in Extended Data Fig. 8. When testing the effects of anomalous HVV couplings, we perform fits to the data with all BSM couplings set to zero, except the one being tested, in the model to be fit. Because the only remaining degree of freedom is the ratio of these BSM couplings to the SM-like coupling, a_1, the probability densities are parametrized in terms of the effective, signed on-shell cross section fraction f_{ai} for each of the a_i coupling, where the sign of the phase of a_i relative to a_1 is absorbed into the definition of f_{ai} [23]. The constraints on Γ_H are found to be stable within 1 MeV (0.1 MeV) for the upper (lower) limits under the different anomalous HVV coupling conditions, and they are summarized in Extended Data Table 1.

In addition, we provide a simplified illustration for the exclusion of the no off-shell hypothesis in Extended Data Fig. 9. In this figure, the total number of events in each bin of the likelihood are compared from the $2\ell2\nu$ and 4ℓ off-shell regions for the fit of the data to the no off-shell ($N_{\text{no off-shell}}$) scenario, and the best fit ($N_{\text{best fit}}$). Events can then be rebinned over the ratio $N_{\text{no off-shell}}/(N_{\text{no off-shell}} + N_{\text{best fit}})$ extracted from each bin, and these rebinned distributions can then be compared at different Γ_H values. In particular, we compare the observed and expected event distributions over this ratio under the best fit scenario, and the scenario with no off-shell H boson production, in order to illustrate which bins bring most sensitivity to the exclusion of the no off-shell scenario. The exclusion is noted to be most apparent from the last two bins displayed in this figure. We note, however, that the full power of the analysis ultimately comes from the different bins over the multidimensional likelihood, and that this figure only serves to condense the information for illustration.

When we perform separate likelihood scans over the three f_{ai} fractions, only the corresponding BSM parameter is allowed to be nonzero in the fit. Profile likelihood scans for f_{a2}, f_{a3} and $f_{\Lambda1}$ under different fit conditions are shown in Extended Data Fig. 8, and the summary of the allowed intervals at 68% and 95% CL is presented in Extended Data Table 1.

Data availability

Tabulated results are provided in the HEPData record for this analysis [38]. Release and preservation of data used by the CMS collaboration as the basis for publications is guided by the CMS data preservation, reuse, and open acess policy.

Code availability

The CMS core software is publicly available on GitHub (https://github.com/cms-sw/cmssw).

Extended Data Table 1: **Results on Γ_{H} and the different anomalous HVV couplings.** The results on Γ_{H} are displayed in units of MeV, and those on the anomalous HVV couplings are summarized in terms of the corresponding on-shell cross section fractions f_{a2}, f_{a3}, and $f_{\Lambda 1}$ (f_{ai} in short, and scaled by 10^5). For the results on Γ_{H}, the tests with the anomalous HVV couplings are distinguished by the denoted f_{ai}, and the expected best-fit values, not quoted explicitly in the table, are always $\Gamma_{\mathrm{H}} = 4.1$ MeV. The SM-like result is the same as that from the combination of all 4ℓ and $2\ell 2\nu$ data sets in Table 1. For the results on f_{ai}, the constraints are shown with either $\Gamma_{\mathrm{H}} = \Gamma_{\mathrm{H}}^{\mathrm{SM}} = 4.1$ MeV required, or Γ_{H} left unconstrained, and the expected best-fit values, also not quoted explicitly, are always null. The various fit conditions are indicated in the column labeled "Condition", where the abbreviation "(u)" indicates which parameter is unconstrained.

Parameter	Condition		Observed		Expected	
		Best fit	68% CL	95% CL	68% CL	95% CL
Γ_{H} (MeV)	SM-like	3.2	$[1.5, 5.6]$	$[0.5, 8.5]$	$[0.6, 8.1]$	$[0.03, 11.3]$
	f_{a2} (u)	3.4	$[1.6, 5.7]$	$[0.6, 8.4]$	$[0.5, 8.0]$	$[0.02, 11.3]$
	f_{a3} (u)	2.7	$[1.3, 4.8]$	$[0.5, 7.3]$	$[0.5, 8.0]$	$[0.02, 11.3]$
	$f_{\Lambda 1}$ (u)	2.7	$[1.3, 4.8]$	$[0.5, 7.3]$	$[0.6, 8.1]$	$[0.02, 11.3]$
f_{a2} ($\times 10^5$)	$\Gamma_{\mathrm{H}} = \Gamma_{\mathrm{H}}^{\mathrm{SM}}$	79	$[6.6, 225]$	$[-32, 514]$	$[-78, 70]$	$[-359, 311]$
	Γ_{H} (u)	72	$[2.7, 216]$	$[-38, 503]$	$[-82, 73]$	$[-413, 364]$
f_{a3} ($\times 10^5$)	$\Gamma_{\mathrm{H}} = \Gamma_{\mathrm{H}}^{\mathrm{SM}}$	2.2	$[-6.4, 32]$	$[-46, 107]$	$[-55, 55]$	$[-198, 198]$
	Γ_{H} (u)	2.4	$[-6.2, 33]$	$[-46, 110]$	$[-58, 58]$	$[-225, 225]$
$f_{\Lambda 1}$ ($\times 10^5$)	$\Gamma_{\mathrm{H}} = \Gamma_{\mathrm{H}}^{\mathrm{SM}}$	2.9	$[-0.62, 17]$	$[-11, 46]$	$[-11, 20]$	$[-47, 68]$
	Γ_{H} (u)	3.1	$[-0.56, 18]$	$[-10, 47]$	$[-11, 21]$	$[-48, 75]$
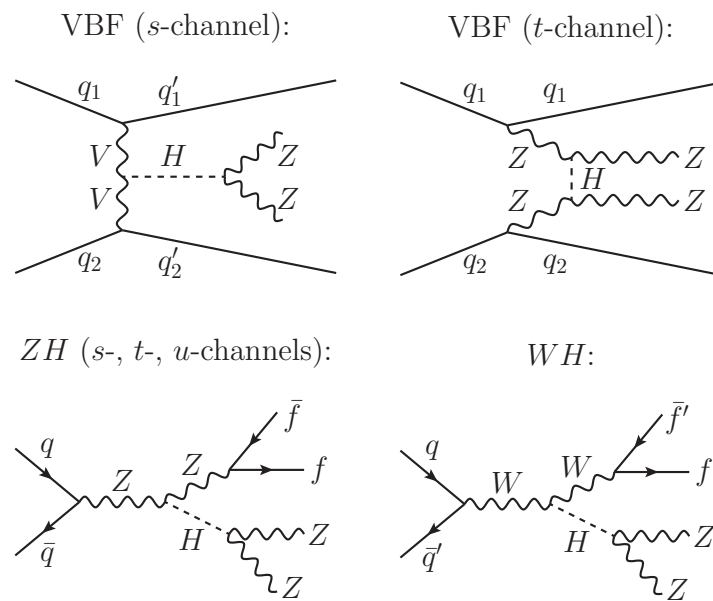
Extended Data Figure 1: **Feynman diagrams for the H boson-mediated EW ZZ production contributions.** Here, f refers to any ℓ, ν, or q. The tree-level diagrams featuring VBF production are grouped together in the upper row, and those featuring VH production are grouped in the lower row. The interaction displayed in each diagram is meant to progress from left to right. Each straight, curvy, or curly line refers to the different set of particles denoted. Straight, solid lines with no arrows indicate the line could refer to either a particle or an antiparticle, whereas those with forward (backward) arrows refer to a particle (an antiparticle).
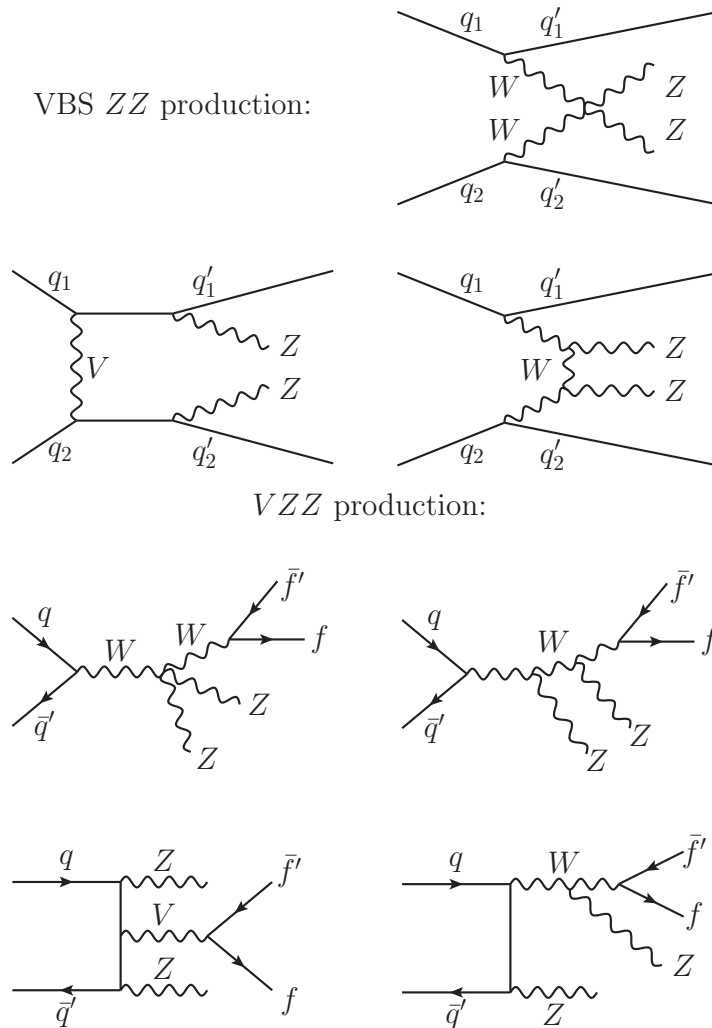
Extended Data Figure 2: **Feynman diagrams for the EW continuum ZZ production contributions.** Here, f refers to any ℓ, ν, or q. The tree-level diagrams featuring vector boson scattering (VBS) production are grouped together in the upper half, and those featuring VZZ production are grouped in the lower half. The interaction displayed in each diagram is meant to progress from left to right. Each straight, curvy, or curly line refers to the different set of particles denoted. Straight, solid lines with no arrows indicate the line could refer to either a particle or an antiparticle, whereas those with forward (backward) arrows refer to a particle (an antiparticle).

$$q\bar{q}' \rightarrow VZ:$$
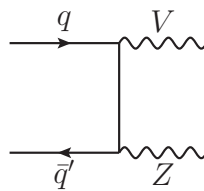
Extended Data Figure 3: **Feynman diagram for the q$\overline{\text{q}}$ $\rightarrow$ ZZ and q$\overline{\text{q}}'$ $\rightarrow$ WZ processes.** Both processes are represented at tree level with a single diagram. These two processes constitute the major irreducible, noninterfering background contributions in the off-shell region. The interaction displayed in each diagram is meant to progress from left to right. Each straight, curvy, or curly line refers to the different set of particles denoted. Straight, solid lines with no arrows indicate the line could refer to either a particle or an antiparticle, whereas those with forward (backward) arrows refer to a particle (an antiparticle).
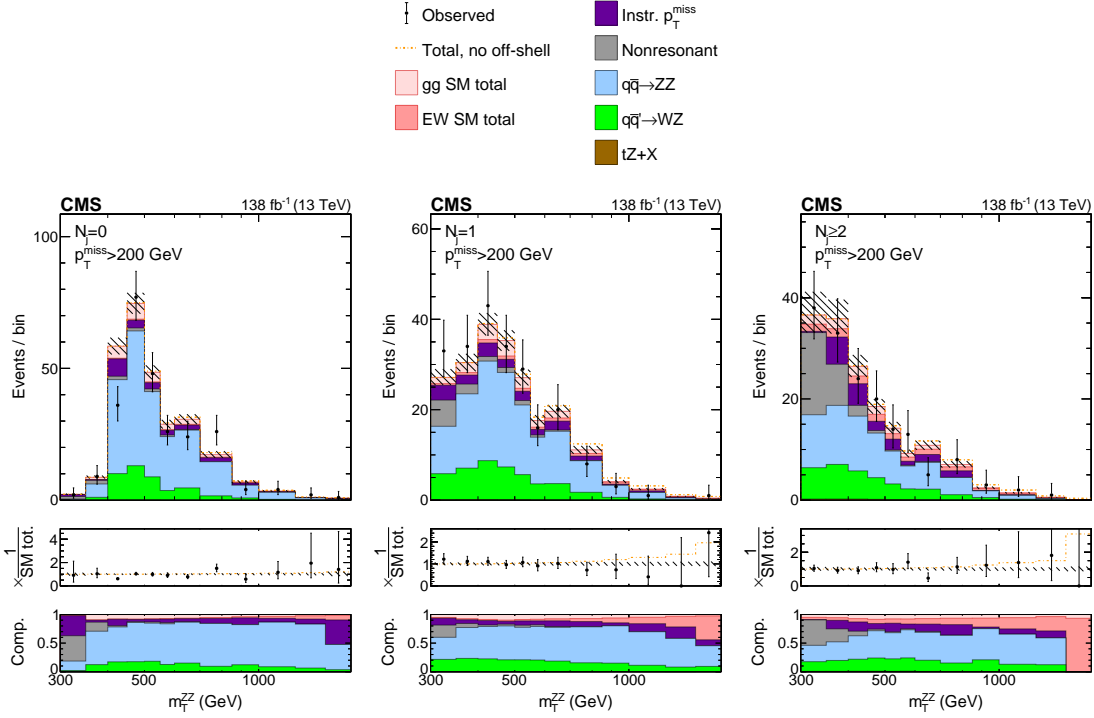
Extended Data Figure 4: **Distributions of m_T^{ZZ} in the different N_j categories of the $2\ell2\nu$ signal region.** The postfit distributions of the transverse ZZ invariant mass are displayed in the jet multiplicity categories of $N_j = 0$ (left), $= 1$ (middle), and ≥ 2 (right) with a missing transverse momentum requirement of $p_T^{miss} > 200$ GeV to enrich H boson contributions. The color legend for the stacked or dot-dashed histograms is given above the plots. The stacked histogram is split into the following components: gg (light pink) and EW (dark pink) ZZ production, instrumental p_T^{miss} background (purple), nonresonant proceses (gray), the $q\overline{q} \to ZZ$ (blue) and $q\overline{q}' \to WZ$ (green) processes, and tZ+X production, where X refers to any other particle. Postfit refers to individual fits of the data (shown as black points with error bars as uncertainties at 68% CL) to the combined $2\ell2\nu + 4\ell$ sample, including the WZ control region, and assuming either SM H boson parameters (stacked histogram with the hashed band as the total postfit uncertainty at 68% CL) or no off-shell H boson production (dot-dashed gold line). The middle panels along the vertical show the ratio of the data or dashed histograms to the stacked histogram, and the lower panels show the predicted relative contributions of each process. The rightmost bins contain the overflow.
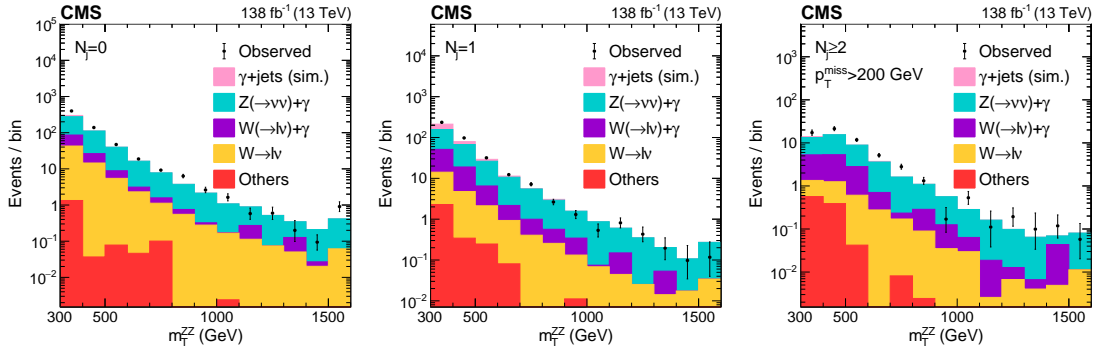
Extended Data Figure 5: **Distributions of m_T^{ZZ} in the different N_j categories of the γ+jets CR.** The distributions of the transverse ZZ invariant mass are displayed for the $N_j = 0$, $N_j = 1$, and $N_j \geq 2$ jet multiplicity categories from left to right. The missing transverse momentum requirement $p_T^{miss} > 200\,\text{GeV}$ is applied in the $N_j \geq 2$ category to focus on the region more sensitive to off-shell H boson production. The stacked histogram shows the predictions for contributions with genuine, large p_T^{miss}, or the instrumental p_T^{miss} background from the γ+jets simulation. Contributions with genuine, large p_T^{miss} are split as those coming from the more dominant $Z(\to \nu\nu)\gamma$ (teal), $W(\to \ell\nu)\gamma$ (purple), and $W(\to \ell\nu)$+jets (yellow) processes, and other small components (red). The prediction for instrumental p_T^{miss} background from simulation is shown in light pink. The black points with error bars as uncertainties at 68% CL show the observed CR data. The distributions are reweighted with the $\gamma \to \ell\ell$ transfer factors extracted from the $p_T^{miss} < 125\,\text{GeV}$ sidebands. The rightmost bins include the overflow. In these distributions, we find a discrepancy between the observed data and the predicted distributions because the reweighted γ+jets samples have inaccurate p_T^{miss} response and the simulation is at LO in QCD. Therefore, we use the difference between the observed data and the genuine-p_T^{miss} contributions to model the instrumental p_T^{miss} background instead of using simulation for this estimate.
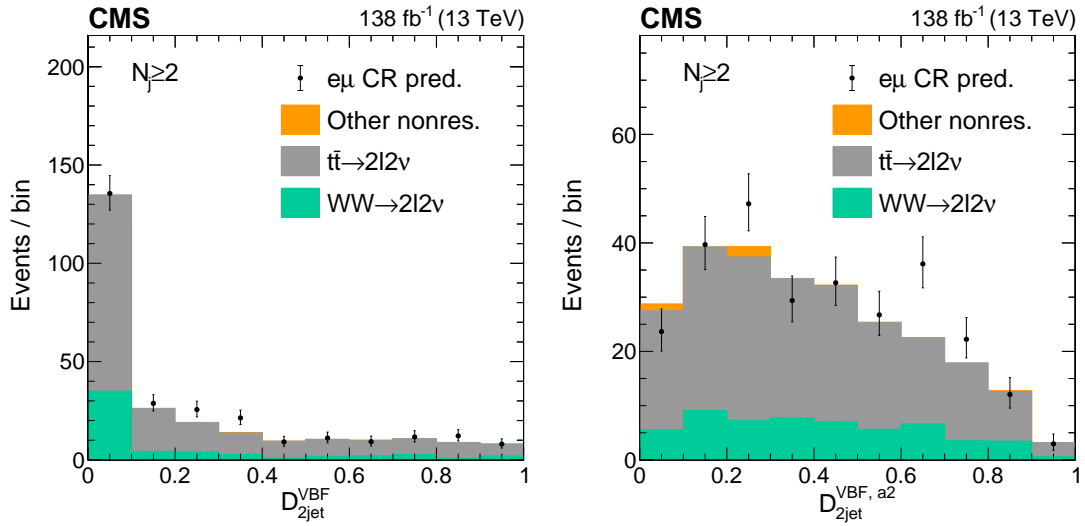
Extended Data Figure 6: **Distributions of the VBF discriminants for nonresonant background.** The distributions of the SM $\mathcal{D}_{2jet}^{VBF}$ (left) and $\mathcal{D}_{2jet}^{VBF,a2}$ (right) kinematic VBF discriminants are shown in the $2\ell2\nu$ signal region, $N_j \geq 2$ category. The stacked histogram shows the predictions from simulation, which consists of nonresonant contributions from WW (green) and $t\bar{t}$ (gray) production, or other small components (orange). The black points with error bars as uncertainties at 68% CL show the prediction from the eμ CR data. While only the data is used in the final estimate of the nonresonant background, we note that predictions from simulation already agree well with the data estimate.
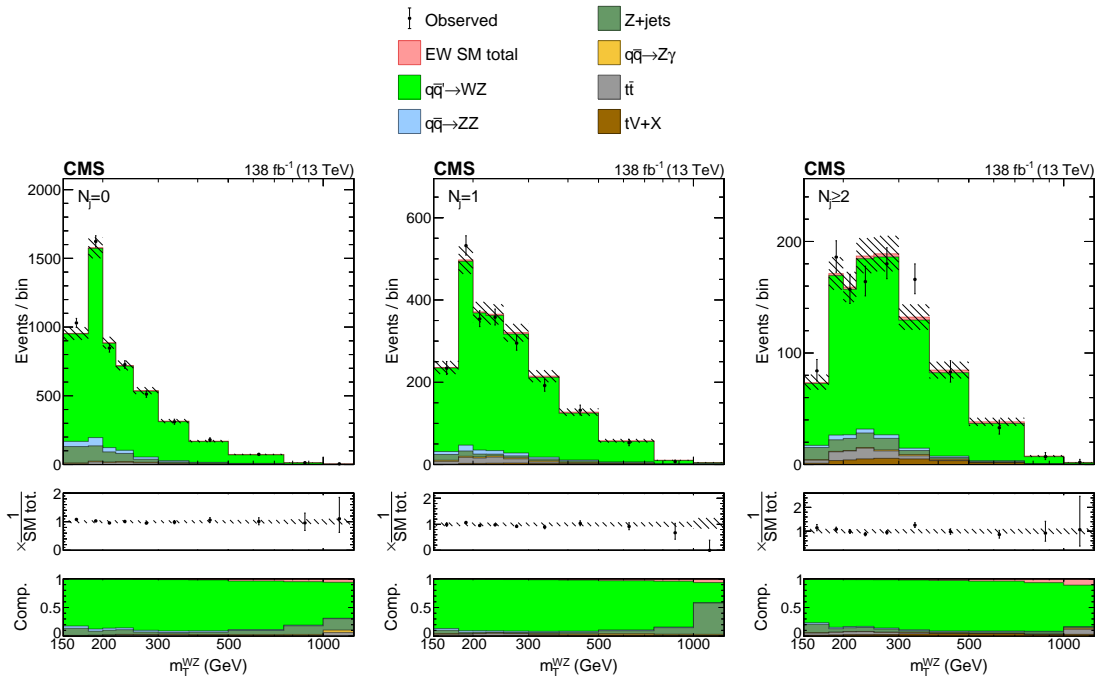
Extended Data Figure 7: **Distributions of m_T^{WZ} in different N_j categories of the WZ control region.** The postfit distributions of the transverse WZ invariant mass are displayed for the $N_j = 0$, $N_j = 1$, and $N_j \geq 2$ jet multiplicity categories of the WZ $\to 3\ell 1\nu$ control region from left to right. Postfit refers to a combined $2\ell 2\nu + 4\ell$ fit, together with this control region, assuming SM H boson parameters. The stacked histogram is shown with the hashed band as the total postfit uncertainty at 68% CL. The color legend is given above the plots, with the different contributions referring to the WZ (light green), ZZ (blue), Z+jets (dark green), $Z\gamma$ (yellow), $t\bar{t}$ (gray), and tV+X (brown, with X being any other particle) production processes, as well as the small EW ZZ production component (dark pink). The black points with error bars as uncertainties at 68% CL show the observed data. The middle panels along the vertical show the ratio of the data to the total prediction, and the lower panels show the predicted relative contributions of each process. The rightmost bins contain the overflow.
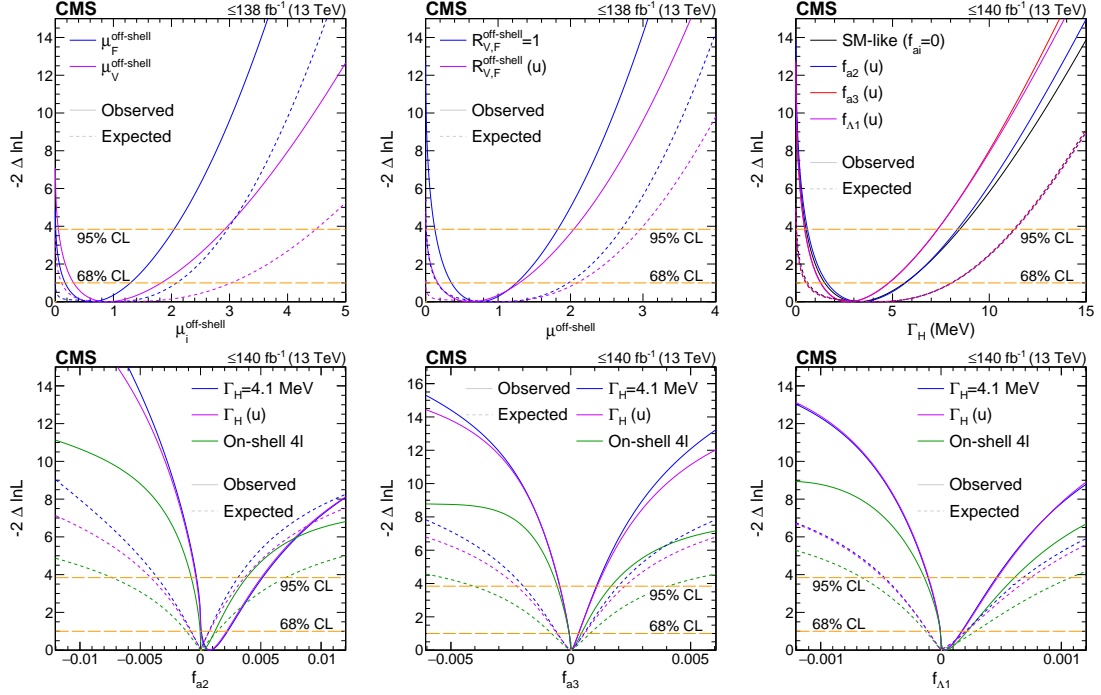
Extended Data Figure 8: **Log-likelihood scans of the off-shell signal strengths, Γ_H, and f_{ai}.**
Top panels: The likelihood scans are shown for $\mu_F^{\text{off-shell}}$ or $\mu_V^{\text{off-shell}}$ (left), $\mu^{\text{off-shell}}$ (middle), and Γ_H (right). Scans for $\mu_F^{\text{off-shell}}$ (blue) and $\mu_V^{\text{off-shell}}$ (magenta) are obtained with the other parameter unconstrained. Those for $\mu^{\text{off-shell}}$ are shown with (blue) and without (magenta) the constraint $R_{V,F}^{\text{off-shell}}(=\mu_V^{\text{off-shell}}/\mu_F^{\text{off-shell}}) = 1$. Constraints on Γ_H are shown with and without anomalous HVV couplings. Bottom panels: The likelihood scans of the anomalous HVV coupling parameters f_{a2} (left), f_{a3} (middle), and $f_{\Lambda 1}$ (right) are shown with the constraint $\Gamma_H = \Gamma_H^{\text{SM}} = 4.1\,\text{MeV}$ (blue), Γ_H unconstrained (magenta), or based on on-shell 4ℓ data only (green). Observed (expected) scans are shown with solid (dashed) curves. The horizontal lines indicate the 68% ($-2\Delta\ln\mathcal{L} = 1.0$) and 95% ($-2\Delta\ln\mathcal{L} = 3.84$) CL regions. The integrated luminosity reaches up to $138\,\text{fb}^{-1}$ when only off-shell information is used, and up to $140\,\text{fb}^{-1}$ when on-shell 4ℓ events are included.
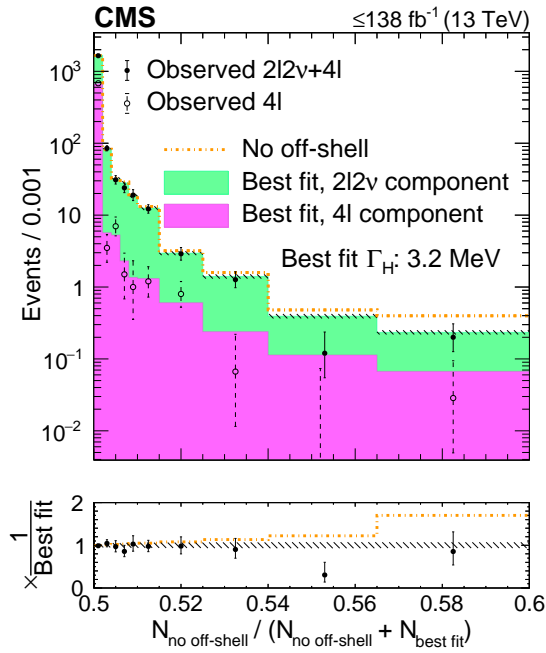
Extended Data Figure 9: **Distributions of ratios of the numbers of events in each off-shell signal region bin.** The ratios are taken after separate fits to the no off-shell hypothesis ($N_{\text{no off-shell}}$) and the best overall fit ($N_{\text{best fit}}$) with the observed Γ_{H} value of 3.2 MeV in the SM-like HVV couplings scenario. The stacked histogram displays the predicted contributions (pink from the 4ℓ off-shell and green from the $2\ell2\nu$ off-shell signal regions) after the best fit, with the hashed band representing the total postfit uncertainty at 68% CL, and the gold dot-dashed line shows the predicted distribution of these ratios for a fit to the no off-shell hypothesis. The black solid (hollow) points, with error bars as uncertainties at 68% CL, represent the observed $2\ell2\nu$ and 4ℓ (4ℓ-only) data. The first and last bins contain the underflow and the overflow, respectively. The bottom panel displays the ratio of the various displayed hypotheses or observed data to the prediction from the best fit. The integrated luminosity reaches only up to $138\,\text{fb}^{-1}$ since on-shell 4ℓ events are not displayed.

Acknowledgments

1 The CMS Collaboration

Yerevan Physics Institute, Yerevan, Armenia

A. Tumasyan

Institut für Hochenergiephysik, Vienna, Austria

W. Adam (iD), J.W. Andrejkovic, T. Bergauer (iD), S. Chatterjee (iD), K. Damanakis, M. Dragicevic (iD), A. Escalante Del Valle (iD), R. Frühwirth[1], M. Jeitler[1] (iD), N. Krammer, L. Lechner (iD), D. Liko, I. Mikulec, P. Paulitsch, F.M. Pitters, J. Schieck[1] (iD), R. Schöfbeck (iD), D. Schwarz, S. Templ (iD), W. Waltenberger (iD), C.-E. Wulz[1] (iD)
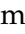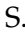
Institute for Nuclear Problems, Minsk, Belarus

V. Chekhovsky, A. Litomin, V. Makarenko (iD)
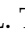
Universiteit Antwerpen, Antwerpen, Belgium

M.R. Darwish[2], E.A. De Wolf, T. Janssen (iD), T. Kello[3], A. Lelek (iD), H. Rejeb Sfar, P. Van Mechelen (iD), S. Van Putte, N. Van Remortel (iD)

Vrije Universiteit Brussel, Brussel, Belgium

E.S. Bols (iD), J. D'Hondt (iD), A. De Moor, M. Delcourt, H. El Faham (iD), S. Lowette (iD), S. Moortgat (iD), A. Morton (iD), D. Müller (iD), A.R. Sahasransu (iD), S. Tavernier (iD), W. Van Doninck, D. Vannerom (iD)

Université Libre de Bruxelles, Bruxelles, Belgium

D. Beghin, B. Bilin (iD), B. Clerbaux (iD), G. De Lentdecker, L. Favart (iD), A.K. Kalsi (iD), K. Lee, M. Mahdavikhorrami, I. Makarenko (iD), S. Paredes (iD), L. Pétré, A. Popov (iD), N. Postiau, E. Starling (iD), L. Thomas (iD), M. Vanden Bemden, C. Vander Velde (iD), P. Vanlaer (iD)

Ghent University, Ghent, Belgium

T. Cornelis (iD), D. Dobur, J. Knolle (iD), L. Lambrecht, G. Mestdach, M. Niedziela (iD), C. Rendón, C. Roskas, A. Samalan, K. Skovpen (iD), M. Tytgat (iD), N. Van Den Bossche, B. Vermassen, L. Wezenbeek
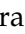
Université Catholique de Louvain, Louvain-la-Neuve, Belgium

A. Benecke, A. Bethani (iD), G. Bruno, F. Bury (iD), C. Caputo (iD), P. David (iD), C. Delaere (iD), I.S. Donertas (iD), A. Giammanco (iD), K. Jaffel, Sa. Jain (iD), V. Lemaitre, K. Mondal (iD), J. Prisciandaro, A. Taliercio, M. Teklishyn (iD), T.T. Tran, P. Vischia (iD), S. Wertz (iD)

Centro Brasileiro de Pesquisas Fisicas, Rio de Janeiro, Brazil

G.A. Alves (iD), C. Hensel, A. Moraes (iD), P. Rebello Teles (iD)

Universidade do Estado do Rio de Janeiro, Rio de Janeiro, Brazil

W.L. Aldá Júnior (iD), M. Alves Gallo Pereira (iD), M. Barroso Ferreira Filho, H. Brandao Malbouisson, W. Carvalho (iD), J. Chinellato[4], E.M. Da Costa (iD), G.G. Da Silveira[5] (iD), D. De Jesus Damiao (iD), V. Dos Santos Sousa, S. Fonseca De Souza (iD), C. Mora Herrera (iD), K. Mota Amarilo, L. Mundim (iD), H. Nogima, A. Santoro, S.M. Silva Do Amaral (iD), A. Sznajder (iD), M. Thiel, F. Torres Da Silva De Araujo[6] (iD), A. Vilela Pereira (iD)

Universidade Estadual Paulista (a), Universidade Federal do ABC (b), São Paulo, Brazil

C.A. Bernardes[5] (iD), L. Calligaris (iD), T.R. Fernandez Perez Tomei (iD), E.M. Gregores (iD), D.S. Lemos (iD), P.G. Mercadante (iD), S.F. Novaes (iD), Sandra S. Padula (iD)

Institute for Nuclear Research and Nuclear Energy, Bulgarian Academy of Sciences, Sofia, Bulgaria

A. Aleksandrov, G. Antchev (iD), R. Hadjiiska, P. Iaydjiev, M. Misheva, M. Rodozov, M. Shopova,

G. Sultanov

University of Sofia, Sofia, Bulgaria
A. Dimitrov, T. Ivanov, L. Litov [iD], B. Pavlov, P. Petkov, A. Petrov
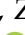
Beihang University, Beijing, China
T. Cheng [iD], T. Javaid[7], M. Mittal, H. Wang[3], L. Yuan

Department of Physics, Tsinghua University, Beijing, China
M. Ahmad [iD], G. Bauer, C. Dozen[8] [iD], Z. Hu [iD], J. Martins[9] [iD], Y. Wang, K. Yi[10,11]

Institute of High Energy Physics, Beijing, China
E. Chapon [iD], G.M. Chen[7] [iD], H.S. Chen[7] [iD], M. Chen [iD], F. Iemmi, A. Kapoor [iD], D. Leggat, H. Liao, Z.-A. Liu[7] [iD], V. Milosevic [iD], F. Monti [iD], R. Sharma [iD], J. Tao [iD], J. Thomas-Wilsker, J. Wang [iD], H. Zhang [iD], J. Zhao [iD]

State Key Laboratory of Nuclear Physics and Technology, Peking University, Beijing, China
A. Agapitos, Y. An, Y. Ban, C. Chen, A. Levin [iD], Q. Li [iD], X. Lyu, Y. Mao, S.J. Qian, D. Wang [iD], J. Xiao, H. Yang

Sun Yat-Sen University, Guangzhou, China
M. Lu, Z. You [iD]

Institute of Modern Physics and Key Laboratory of Nuclear Physics and Ion-beam Application (MOE) - Fudan University, Shanghai, China
X. Gao[3], H. Okawa [iD], Y. Zhang [iD]

Zhejiang University, Hangzhou, China, Zhejiang, China
Z. Lin [iD], M. Xiao [iD]

Universidad de Los Andes, Bogota, Colombia
C. Avila [iD], A. Cabrera [iD], C. Florez [iD], J. Fraga

Universidad de Antioquia, Medellin, Colombia
J. Mejia Guisao, F. Ramirez, J.D. Ruiz Alvarez [iD]

University of Split, Faculty of Electrical Engineering, Mechanical Engineering and Naval Architecture, Split, Croatia
D. Giljanovic, N. Godinovic [iD], D. Lelas [iD], I. Puljak [iD]

University of Split, Faculty of Science, Split, Croatia
Z. Antunovic, M. Kovac, T. Sculac [iD]

Institute Rudjer Boskovic, Zagreb, Croatia
V. Brigljevic [iD], D. Ferencek [iD], D. Majumder [iD], M. Roguljic, A. Starodumov[12] [iD], T. Susa [iD]

University of Cyprus, Nicosia, Cyprus
A. Attikis [iD], K. Christoforou, G. Kole [iD], M. Kolosova, S. Konstantinou, J. Mousa [iD], C. Nicolaou, F. Ptochos [iD], P.A. Razis, H. Rykaczewski, H. Saka [iD]

Charles University, Prague, Czech Republic
M. Finger[13], M. Finger Jr.[13] [iD], A. Kveton

Escuela Politecnica Nacional, Quito, Ecuador
E. Ayala

Universidad San Francisco de Quito, Quito, Ecuador
E. Carrera Jarrin [iD]

Academy of Scientific Research and Technology of the Arab Republic of Egypt, Egyptian Network of High Energy Physics, Cairo, Egypt

H. Abdalla[14] (iD), E. Salama[15,16]

Center for High Energy Physics (CHEP-FU), Fayoum University, El-Fayoum, Egypt

M.A. Mahmoud (iD), Y. Mohammed (iD)

National Institute of Chemical Physics and Biophysics, Tallinn, Estonia

S. Bhowmik (iD), R.K. Dewanjee (iD), K. Ehataht, M. Kadastik, S. Nandan, C. Nielsen, J. Pata, M. Raidal (iD), L. Tani, C. Veelken

Department of Physics, University of Helsinki, Helsinki, Finland

P. Eerola (iD), H. Kirschenmann (iD), K. Osterberg (iD), M. Voutilainen (iD)

Helsinki Institute of Physics, Helsinki, Finland

S. Bharthuar, E. Brücken (iD), F. Garcia (iD), J. Havukainen (iD), M.S. Kim (iD), R. Kinnunen, T. Lampén, K. Lassila-Perini (iD), S. Lehti (iD), T. Lindén, M. Lotti, L. Martikainen, M. Myllymäki, J. Ott (iD), M.m. Rantanen, H. Siikonen, E. Tuominen (iD), J. Tuominiemi
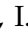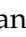
Lappeenranta University of Technology, Lappeenranta, Finland

P. Luukka (iD), H. Petrow, T. Tuuva

IRFU, CEA, Université Paris-Saclay, Gif-sur-Yvette, France

C. Amendola (iD), M. Besancon, F. Couderc (iD), M. Dejardin, D. Denegri, J.L. Faure, F. Ferri (iD), S. Ganjour, P. Gras, G. Hamel de Monchenault (iD), P. Jarry, B. Lenzi (iD), J. Malcles, J. Rander, A. Rosowsky (iD), M.Ö. Sahin (iD), A. Savoy-Navarro[17], P. Simkina, M. Titov (iD), G.B. Yu (iD)
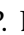
Laboratoire Leprince-Ringuet, CNRS/IN2P3, Ecole Polytechnique, Institut Polytechnique de Paris, Palaiseau, France

S. Ahuja (iD), F. Beaudette (iD), M. Bonanomi (iD), A. Buchot Perraguin, P. Busson, A. Cappati, C. Charlot, O. Davignon, B. Diab, G. Falmagne (iD), B.A. Fontana Santos Alves, S. Ghosh, R. Granier de Cassagnac (iD), A. Hakimi, I. Kucher (iD), J. Motta, M. Nguyen (iD), C. Ochando (iD), P. Paganini (iD), J. Rembser, R. Salerno (iD), U. Sarkar (iD), J.B. Sauvan (iD), Y. Sirois (iD), A. Tarabini, A. Zabi, A. Zghiche (iD)

Université de Strasbourg, CNRS, IPHC UMR 7178, Strasbourg, France

J.-L. Agram[18] (iD), J. Andrea, D. Apparu, D. Bloch (iD), G. Bourgatte, J.-M. Brom, E.C. Chabert, C. Collard (iD), D. Darej, J.-C. Fontaine[18], U. Goerlach, C. Grimault, A.-C. Le Bihan, E. Nibigira (iD), P. Van Hove (iD)

Institut de Physique des 2 Infinis de Lyon (IP2I), Villeurbanne, France

E. Asilar (iD), S. Beauceron (iD), C. Bernet (iD), G. Boudoul, C. Camen, A. Carle, N. Chanon (iD), D. Contardo, P. Depasse (iD), H. El Mamouni, J. Fay, S. Gascon (iD), M. Gouzevitch (iD), B. Ille, I.B. Laktineh, H. Lattaud (iD), A. Lesauvage (iD), M. Lethuillier (iD), L. Mirabito, S. Perries, K. Shchablo, V. Sordini (iD), G. Touquet, M. Vander Donckt, S. Viret

Georgian Technical University, Tbilisi, Georgia

I. Lomidze, T. Toriashvili[19], Z. Tsamalaidze[13]

RWTH Aachen University, I. Physikalisches Institut, Aachen, Germany

V. Botta, L. Feld (iD), K. Klein, M. Lipinski, D. Meuser, A. Pauls, N. Röwert, J. Schulz, M. Teroerde (iD)

RWTH Aachen University, III. Physikalisches Institut A, Aachen, Germany
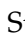
A. Dodonova, D. Eliseev, M. Erdmann (iD), P. Fackeldey (iD), B. Fischer, T. Hebbeker (iD),

K. Hoepfner, F. Ivone, L. Mastrolorenzo, M. Merschmeyer, A. Meyer, G. Mocellin, S. Mondal, S. Mukherjee, D. Noll, A. Novak, A. Pozdnyakov, Y. Rath, H. Reithler, A. Schmidt, S.C. Schuler, A. Sharma, L. Vigilante, S. Wiedenbeck, S. Zaleski
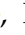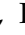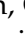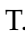
RWTH Aachen University, III. Physikalisches Institut B, Aachen, Germany
C. Dziwok, G. Flügge, W. Haj Ahmad[20], O. Hlushchenko, T. Kress, A. Nowack, O. Pooth, D. Roy, A. Stahl[21], T. Ziemons, A. Zotz
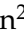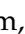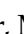
Deutsches Elektronen-Synchrotron, Hamburg, Germany
H. Aarup Petersen, M. Aldaya Martin, P. Asmuss, S. Baxter, M. Bayatmakou, O. Behnke, A. Bermúdez Martínez, S. Bhattacharya, A.A. Bin Anuar, F. Blekman[22], K. Borras[23], D. Brunner, A. Campbell, A. Cardini, C. Cheng, F. Colombina, S. Consuegra Rodríguez, G. Correia Silva, M. De Silva, L. Didukh, G. Eckerlin, D. Eckstein, L.I. Estevez Banos, O. Filatov, E. Gallo[22], A. Geiser, A. Giraldi, G. Greau, A. Grohsjean, M. Guthoff, A. Jafari[24], N.Z. Jomhari, H. Jung, A. Kasem[23], M. Kasemann, H. Kaveh, C. Kleinwort, R. Kogler, D. Krücker, W. Lange, K. Lipka, W. Lohmann[25], R. Mankel, I.-A. Melzer-Pellmann, M. Mendizabal Morentin, J. Metwally, A.B. Meyer, M. Meyer, J. Mnich, A. Mussgiller, A. Nürnberg, Y. Otarid, D. Pérez Adán, D. Pitzl, A. Raspereza, B. Ribeiro Lopes, J. Rübenach, A. Saggio, A. Saibel, M. Savitskyi, M. Scham[26], V. Scheurer, S. Schnake, P. Schütze, C. Schwanenberger[22], M. Shchedrolosiev, R.E. Sosa Ricardo, D. Stafford, N. Tonon, M. Van De Klundert, F. Vazzoler, R. Walsh, D. Walter, Q. Wang, Y. Wen, K. Wichmann, L. Wiens, C. Wissing, S. Wuchterl

University of Hamburg, Hamburg, Germany
R. Aggleton, S. Albrecht, S. Bein, L. Benato, P. Connor, K. De Leo, M. Eich, K. El Morabit, F. Feindt, A. Fröhlich, C. Garbers, E. Garutti, P. Gunnellini, M. Hajheidari, J. Haller, A. Hinzmann, G. Kasieczka, R. Klanner, T. Kramer, V. Kutzner, J. Lange, T. Lange, A. Lobanov, A. Malara, C. Matthies, A. Mehta, L. Moureaux, A. Nigamova, K.J. Pena Rodriguez, M. Rieger, O. Rieger, P. Schleper, M. Schröder, J. Schwandt, J. Sonneveld, H. Stadie, G. Steinbrück, A. Tews, I. Zoi

Karlsruher Institut fuer Technologie, Karlsruhe, Germany
J. Bechtel, S. Brommer, M. Burkart, E. Butz, R. Caspart, T. Chwalek, W. De Boer[+], A. Dierlamm, A. Droll, N. Faltermann, M. Giffels, J.O. Gosewisch, A. Gottmann, F. Hartmann[21], C. Heidecker, U. Husemann, P. Keicher, R. Koppenhöfer, S. Maier, S. Mitra, Th. Müller, M. Neukum, G. Quast, K. Rabbertz, J. Rauser, D. Savoiu, M. Schnepf, D. Seith, I. Shvetsov, H.J. Simonis, R. Ulrich, J. Van Der Linden, R.F. Von Cube, M. Wassmer, M. Weber, S. Wieland, R. Wolf, S. Wozniewski, S. Wunsch

Institute of Nuclear and Particle Physics (INPP), NCSR Demokritos, Aghia Paraskevi, Greece
G. Anagnostou, G. Daskalakis, A. Kyriakis, D. Loukas, A. Stakia

National and Kapodistrian University of Athens, Athens, Greece
M. Diamantopoulou, D. Karasavvas, P. Kontaxakis, C.K. Koraka, A. Manousakis-Katsikakis, A. Panagiotou, I. Papavergou, N. Saoulidou, K. Theofilatos, E. Tziaferi, K. Vellidis, E. Vourliotis

National Technical University of Athens, Athens, Greece
G. Bakas, K. Kousouris, I. Papakrivopoulos, G. Tsipolitis, A. Zacharopoulou

University of Ioánnina, Ioánnina, Greece

K. Adamidis, I. Bestintzanos, I. Evangelou (iD), C. Foudas, P. Gianneios, P. Katsoulis, P. Kokkas, N. Manthos, I. Papadopoulos (iD), J. Strologas (iD)

MTA-ELTE Lendület CMS Particle and Nuclear Physics Group, Eötvös Loránd University, Budapest, Hungary
M. Csanad (iD), K. Farkas, M.M.A. Gadallah[27] (iD), S. Lökös[28] (iD), P. Major, K. Mandal (iD), G. Pasztor (iD), A.J. Rádl, O. Surányi, G.I. Veres (iD)

Wigner Research Centre for Physics, Budapest, Hungary
M. Bartók[29] (iD), G. Bencze, C. Hajdu (iD), D. Horvath[30,31] (iD), F. Sikler (iD), V. Veszpremi (iD)

Institute of Nuclear Research ATOMKI, Debrecen, Hungary
S. Czellar, D. Fasanella (iD), F. Fienga (iD), J. Karancsi[29] (iD), J. Molnar, Z. Szillasi, D. Teyssier

Institute of Physics, University of Debrecen, Debrecen, Hungary
P. Raics, Z.L. Trocsanyi[32] (iD), B. Ujvari[33]

Karoly Robert Campus, MATE Institute of Technology, Gyongyos, Hungary
T. Csorgo[34] (iD), F. Nemes[34], T. Novak

National Institute of Science Education and Research, HBNI, Bhubaneswar, India
S. Bahinipati[35] (iD), C. Kar (iD), P. Mal, T. Mishra (iD), V.K. Muraleedharan Nair Bindhu[36], A. Nayak[36] (iD), P. Saha, N. Sur (iD), S.K. Swain, D. Vats[36]

Panjab University, Chandigarh, India
S. Bansal (iD), S.B. Beri, V. Bhatnagar (iD), G. Chaudhary (iD), S. Chauhan (iD), N. Dhingra[37] (iD), R. Gupta, A. Kaur, H. Kaur, M. Kaur (iD), P. Kumari (iD), M. Meena, K. Sandeep (iD), J.B. Singh[38] (iD), A.K. Virdi (iD)

University of Delhi, Delhi, India
A. Ahmed, A. Bhardwaj (iD), B.C. Choudhary (iD), M. Gola, S. Keshri (iD), A. Kumar (iD), M. Naimuddin (iD), P. Priyanka (iD), K. Ranjan, S. Saumya, A. Shah (iD)

Saha Institute of Nuclear Physics, HBNI, Kolkata, India
M. Bharti[39], R. Bhattacharya, S. Bhattacharya (iD), D. Bhowmik, S. Dutta, S. Dutta, B. Gomber[40] (iD), M. Maity[41], P. Palit (iD), P.K. Rout (iD), G. Saha, B. Sahu (iD), S. Sarkar, M. Sharan

Indian Institute of Technology Madras, Madras, India
P.K. Behera (iD), S.C. Behera, P. Kalbhor (iD), J.R. Komaragiri[42] (iD), D. Kumar[42], A. Muhammad, L. Panwar[42] (iD), R. Pradhan, P.R. Pujahari, A. Sharma (iD), A.K. Sikdar, P.C. Tiwari[42] (iD)

Bhabha Atomic Research Centre, Mumbai, India
K. Naskar[43]

Tata Institute of Fundamental Research-A, Mumbai, India
T. Aziz, S. Dugad, M. Kumar, G.B. Mohanty (iD)

Tata Institute of Fundamental Research-B, Mumbai, India
S. Banerjee (iD), R. Chudasama, M. Guchait, S. Karmakar, S. Kumar, G. Majumder, K. Mazumdar, S. Mukherjee (iD)
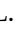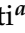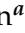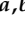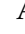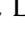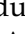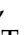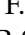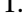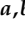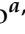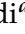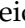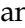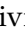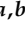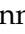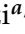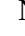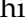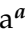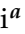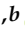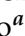
Indian Institute of Science Education and Research (IISER), Pune, India
A. Alpana, S. Dube (iD), B. Kansal, A. Laha, S. Pandey (iD), A. Rastogi (iD), S. Sharma (iD)

Isfahan University of Technology, Isfahan, Iran
H. Bakhshiansohi[44,45] (iD), E. Khazaie[45], M. Zeinali[46]
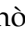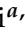
Institute for Research in Fundamental Sciences (IPM), Tehran, Iran
S. Chenarani[47], S.M. Etesami (iD), M. Khakzad (iD), M. Mohammadi Najafabadi (iD)

University College Dublin, Dublin, Ireland
M. Grunewald (iD)

INFN Sezione di Bari *a*, **Bari, Italy, Università di Bari** *b*, **Bari, Italy, Politecnico di Bari** *c*, **Bari, Italy**
M. Abbrescia*a,b* (iD), R. Aly*a,b,48* (iD), C. Aruta*a,b*, A. Colaleo*a* (iD), D. Creanza*a,c* (iD), N. De Filippis*a,c* (iD), M. De Palma*a,b* (iD), A. Di Florio*a,b*, A. Di Pilato*a,b* (iD), W. Elmetenawee*a,b* (iD), F. Errico*a,b* (iD), L. Fiore*a* (iD), G. Iaselli*a,c* (iD), M. Ince*a,b* (iD), S. Lezki*a,b* (iD), G. Maggi*a,c* (iD), M. Maggi*a* (iD), I. Margjeka*a,b*, V. Mastrapasqua*a,b* (iD), S. My*a,b* (iD), S. Nuzzo*a,b* (iD), A. Pellecchia*a,b*, A. Pompili*a,b* (iD), G. Pugliese*a,c* (iD), D. Ramos*a*, A. Ranieri*a* (iD), G. Selvaggi*a,b* (iD), L. Silvestris*a* (iD), F.M. Simone*a,b* (iD), Ü. Sözbilir*a*, R. Venditti*a* (iD), P. Verwilligen*a* (iD)

INFN Sezione di Bologna *a*, **Bologna, Italy, Università di Bologna** *b*, **Bologna, Italy**
G. Abbiendi*a* (iD), C. Battilana*a,b* (iD), D. Bonacorsi*a,b* (iD), L. Borgonovi*a*, L. Brigliadori*a*, R. Campanini*a,b* (iD), P. Capiluppi*a,b* (iD), A. Castro*a,b* (iD), F.R. Cavallo*a* (iD), C. Ciocca*a* (iD), M. Cuffiani*a,b* (iD), G.M. Dallavalle*a*, T. Diotalevi*a,b* (iD), F. Fabbri*a* (iD), A. Fanfani*a,b* (iD), P. Giacomelli*a* (iD), L. Giommi*a,b* (iD), C. Grandi*a* (iD), L. Guiducci*a,b*, S. Lo Meo*a,49*, L. Lunerti*a,b*, S. Marcellini*a* (iD), G. Masetti*a* (iD), F.L. Navarria*a,b* (iD), A. Perrotta*a* (iD), F. Primavera*a,b* (iD), A.M. Rossi*a,b* (iD), T. Rovelli*a,b* (iD), G.P. Siroli*a,b* (iD)

INFN Sezione di Catania *a*, **Catania, Italy, Università di Catania** *b*, **Catania, Italy**
S. Albergo*a,b,50* (iD), S. Costa*a,b,50* (iD), A. Di Mattia*a* (iD), R. Potenza*a,b*, A. Tricomi*a,b,50* (iD), C. Tuve*a,b* (iD)

INFN Sezione di Firenze *a*, **Firenze, Italy, Università di Firenze** *b*, **Firenze, Italy**
G. Barbagli*a* (iD), A. Cassese*a* (iD), R. Ceccarelli*a,b*, V. Ciulli*a,b* (iD), C. Civinini*a* (iD), R. D'Alessandro*a,b* (iD), E. Focardi*a,b* (iD), G. Latino*a,b* (iD), P. Lenzi*a,b* (iD), M. Lizzo*a,b*, M. Meschini*a* (iD), S. Paoletti*a* (iD), R. Seidita*a,b*, G. Sguazzoni*a* (iD), L. Viliani*a* (iD)

INFN Laboratori Nazionali di Frascati, Frascati, Italy
L. Benussi (iD), S. Bianco (iD), D. Piccolo (iD)

INFN Sezione di Genova *a*, **Genova, Italy, Università di Genova** *b*, **Genova, Italy**
M. Bozzo*a,b* (iD), F. Ferro*a* (iD), R. Mulargia*a*, E. Robutti*a* (iD), S. Tosi*a,b* (iD)

INFN Sezione di Milano-Bicocca *a*, **Milano, Italy, Università di Milano-Bicocca** *b*, **Milano, Italy**
A. Benaglia*a* (iD), G. Boldrini (iD), F. Brivio*a,b*, F. Cetorelli*a,b*, F. De Guio*a,b* (iD), M.E. Dinardo*a,b* (iD), P. Dini*a* (iD), S. Gennai*a* (iD), A. Ghezzi*a,b* (iD), P. Govoni*a,b* (iD), L. Guzzi*a,b* (iD), M.T. Lucchini*a,b* (iD), M. Malberti*a*, S. Malvezzi*a* (iD), A. Massironi*a* (iD), D. Menasce*a* (iD), L. Moroni*a* (iD), M. Paganoni*a,b* (iD), D. Pedrini*a* (iD), B.S. Pinolini, S. Ragazzi*a,b* (iD), N. Redaelli*a* (iD), T. Tabarelli de Fatis*a,b* (iD), D. Valsecchi*a,b,21*, D. Zuolo*a,b* (iD)

INFN Sezione di Napoli *a*, **Napoli, Italy, Università di Napoli 'Federico II'** *b*, **Napoli, Italy, Università della Basilicata** *c*, **Potenza, Italy, Università G. Marconi** *d*, **Roma, Italy**
S. Buontempo*a* (iD), F. Carnevali*a,b*, N. Cavallo*a,c* (iD), A. De Iorio*a,b* (iD), F. Fabozzi*a,c* (iD), A.O.M. Iorio*a,b* (iD), L. Lista*a,b,51* (iD), S. Meola*a,d,21* (iD), P. Paolucci*a,21* (iD), B. Rossi*a* (iD), C. Sciacca*a,b* (iD)

INFN Sezione di Padova *a*, **Padova, Italy, Università di Padova** *b*, **Padova, Italy, Università di Trento** *c*, **Trento, Italy**

P. Azzi[a] (iD), N. Bacchetta[a] (iD), D. Bisello[a,b] (iD), P. Bortignon[a] (iD), A. Bragagnolo[a,b] (iD), R. Carlin[a,b] (iD), P. Checchia[a] (iD), T. Dorigo[a] (iD), U. Dosselli[a] (iD), F. Gasparini[a,b] (iD), U. Gasparini[a,b] (iD), G. Grosso, L. Layer[a,52], E. Lusiani (iD), M. Margoni[a,b] (iD), F. Marini, A.T. Meneguzzo[a,b] (iD), J. Pazzini[a,b] (iD), P. Ronchese[a,b] (iD), R. Rossin[a,b], F. Simonetto[a,b] (iD), G. Strong[a] (iD), M. Tosi[a,b] (iD), H. Yarar[a,b], M. Zanetti[a,b] (iD), P. Zotto[a,b] (iD), A. Zucchetta[a,b] (iD), G. Zumerle[a,b] (iD)
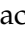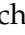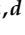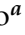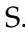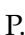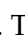
INFN Sezione di Pavia [a], Pavia, Italy, Università di Pavia [b], Pavia, Italy
C. Aimè[a,b], A. Braghieri[a] (iD), S. Calzaferri[a,b], D. Fiorina[a,b] (iD), P. Montagna[a,b], S.P. Ratti[a,b], V. Re[a] (iD), C. Riccardi[a,b] (iD), P. Salvini[a] (iD), I. Vai[a] (iD), P. Vitulo[a,b] (iD)
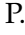
INFN Sezione di Perugia [a], Perugia, Italy, Università di Perugia [b], Perugia, Italy
P. Asenov[a,53] (iD), G.M. Bilei[a] (iD), D. Ciangottini[a,b] (iD), L. Fanò[a,b] (iD), M. Magherini[b], G. Mantovani[a,b], V. Mariani[a,b], M. Menichelli[a] (iD), F. Moscatelli[a,53] (iD), A. Piccinelli[a,b] (iD), M. Presilla[a,b] (iD), A. Rossi[a,b] (iD), A. Santocchia[a,b] (iD), D. Spiga[a] (iD), T. Tedeschi[a,b] (iD)
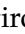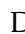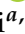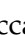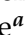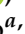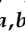
INFN Sezione di Pisa [a], Pisa, Italy, Università di Pisa [b], Pisa, Italy, Scuola Normale Superiore di Pisa [c], Pisa, Italy, Università di Siena [d], Siena, Italy
P. Azzurri[a] (iD), G. Bagliesi[a] (iD), V. Bertacchi[a,c] (iD), L. Bianchini[a] (iD), T. Boccali[a] (iD), E. Bossini[a,b] (iD), R. Castaldi[a] (iD), M.A. Ciocci[a,b] (iD), V. D'Amante[a,d] (iD), R. Dell'Orso[a] (iD), M.R. Di Domenico[a,d] (iD), S. Donato[a] (iD), A. Giassi[a] (iD), F. Ligabue[a,c] (iD), E. Manca[a,c] (iD), G. Mandorli[a,c] (iD), D. Matos Figueiredo, A. Messineo[a,b] (iD), M. Musich[a], F. Palla[a] (iD), S. Parolia[a,b], G. Ramirez-Sanchez[a,c], A. Rizzi[a,b] (iD), G. Rolandi[a,c] (iD), S. Roy Chowdhury[a,c], A. Scribano[a], N. Shafiei[a,b] (iD), P. Spagnolo[a] (iD), R. Tenchini[a] (iD), G. Tonelli[a,b] (iD), N. Turini[a,d] (iD), A. Venturi[a] (iD), P.G. Verdini[a] (iD)
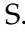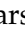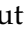
INFN Sezione di Roma [a], Rome, Italy, Sapienza Università di Roma [b], Rome, Italy
P. Barria[a] (iD), M. Campana[a,b], F. Cavallari[a] (iD), D. Del Re[a,b] (iD), E. Di Marco[a] (iD), M. Diemoz[a] (iD), E. Longo[a,b] (iD), P. Meridiani[a] (iD), G. Organtini[a,b] (iD), F. Pandolfi[a], R. Paramatti[a,b] (iD), C. Quaranta[a,b], S. Rahatlou[a,b] (iD), C. Rovelli[a] (iD), F. Santanastasio[a,b] (iD), L. Soffi[a] (iD), R. Tramontano[a,b]
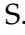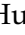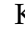
INFN Sezione di Torino [a], Torino, Italy, Università di Torino [b], Torino, Italy, Università del Piemonte Orientale [c], Novara, Italy
N. Amapane[a,b] (iD), R. Arcidiacono[a,c] (iD), S. Argiro[a,b] (iD), M. Arneodo[a,c] (iD), N. Bartosik[a] (iD), R. Bellan[a,b] (iD), A. Bellora[a,b] (iD), J. Berenguer Antequera[a,b] (iD), C. Biino[a] (iD), N. Cartiglia[a] (iD), M. Costa[a,b] (iD), R. Covarelli[a,b] (iD), N. Demaria[a] (iD), M. Grippo[a,b] (iD), B. Kiani[a,b] (iD), F. Legger[a] (iD), C. Mariotti[a] (iD), S. Maselli[a] (iD), A. Mecca[a,b] (iD), E. Migliore[a,b] (iD), E. Monteil[a,b] (iD), M. Monteno[a] (iD), M.M. Obertino[a,b] (iD), G. Ortona[a] (iD), L. Pacher[a,b] (iD), N. Pastrone[a] (iD), M. Pelliccioni[a] (iD), M. Ruspa[a,c] (iD), K. Shchelina[a] (iD), F. Siviero[a,b] (iD), V. Sola[a] (iD), A. Solano[a,b] (iD), D. Soldi[a,b] (iD), A. Staiano[a] (iD), M. Tornago[a,b], D. Trocino[a] (iD), G. Umoret[a,b], A. Vagnerini[a,b]

INFN Sezione di Trieste [a], Trieste, Italy, Università di Trieste [b], Trieste, Italy
S. Belforte[a] (iD), V. Candelise[a,b] (iD), M. Casarsa[a] (iD), F. Cossutti[a] (iD), A. Da Rold[a,b] (iD), G. Della Ricca[a,b] (iD), G. Sorrentino[a,b]

Kyungpook National University, Daegu, Korea
S. Dogra (iD), C. Huh (iD), B. Kim, D.H. Kim (iD), G.N. Kim (iD), J. Kim, J. Lee, S.W. Lee (iD), C.S. Moon (iD), Y.D. Oh (iD), S.I. Pak, S. Sekmen (iD), Y.C. Yang

Chonnam National University, Institute for Universe and Elementary Particles, Kwangju, Korea
H. Kim (iD), D.H. Moon (iD)

Hanyang University, Seoul, Korea

B. Francois (iD), T.J. Kim (iD), J. Park (iD)

Korea University, Seoul, Korea
S. Cho, S. Choi (iD), B. Hong (iD), K. Lee, K.S. Lee (iD), J. Lim, J. Park, S.K. Park, J. Yoo

Kyung Hee University, Department of Physics, Seoul, Republic of Korea, Seoul, Korea
J. Goh (iD), A. Gurtu

Sejong University, Seoul, Korea
H.S. Kim (iD), Y. Kim

Seoul National University, Seoul, Korea
J. Almond, J.H. Bhyun, J. Choi, S. Jeon, J. Kim, J.S. Kim, S. Ko, H. Kwon, H. Lee (iD), S. Lee, B.H. Oh, M. Oh (iD), S.B. Oh, H. Seo (iD), U.K. Yang, I. Yoon (iD)

University of Seoul, Seoul, Korea
W. Jang, D.Y. Kang, Y. Kang, S. Kim, B. Ko, J.S.H. Lee (iD), Y. Lee, J.A. Merlin, I.C. Park, Y. Roh, M.S. Ryu, D. Song, I.J. Watson (iD), S. Yang

Yonsei University, Department of Physics, Seoul, Korea
S. Ha, H.D. Yoo

Sungkyunkwan University, Suwon, Korea
M. Choi, H. Lee, Y. Lee, I. Yu (iD)

College of Engineering and Technology, American University of the Middle East (AUM), Egaila, Kuwait, Dasman, Kuwait
T. Beyrouthy, Y. Maghrbi

Riga Technical University, Riga, Latvia
K. Dreimanis (iD), V. Veckalns[54] (iD)

Vilnius University, Vilnius, Lithuania
M. Ambrozas, A. Carvalho Antunes De Oliveira (iD), A. Juodagalvis (iD), A. Rinkevicius (iD), G. Tamulaitis (iD)

National Centre for Particle Physics, Universiti Malaya, Kuala Lumpur, Malaysia
N. Bin Norjoharuddeen (iD), S.Y. Hoh[55] (iD), Z. Zolkapli

Universidad de Sonora (UNISON), Hermosillo, Mexico
J.F. Benitez (iD), A. Castaneda Hernandez (iD), H.A. Encinas Acosta, L.G. Gallegos Maríñez, M. León Coello, J.A. Murillo Quijada (iD), A. Sehrawat, L. Valencia Palomo (iD)

Centro de Investigacion y de Estudios Avanzados del IPN, Mexico City, Mexico
G. Ayala, H. Castilla-Valdez, E. De La Cruz-Burelo (iD), I. Heredia-De La Cruz[56] (iD), R. Lopez-Fernandez, C.A. Mondragon Herrera, D.A. Perez Navarro, R. Reyes-Almanza (iD), A. Sánchez Hernández (iD)

Universidad Iberoamericana, Mexico City, Mexico
S. Carrillo Moreno, C. Oropeza Barrera (iD), F. Vazquez Valencia

Benemerita Universidad Autonoma de Puebla, Puebla, Mexico
I. Pedraza, H.A. Salazar Ibarguen, C. Uribe Estrada

University of Montenegro, Podgorica, Montenegro
I. Bubanja, J. Mijuskovic[57], N. Raicevic

University of Auckland, Auckland, New Zealand

D. Krofcheck

University of Canterbury, Christchurch, New Zealand
P.H. Butler

National Centre for Physics, Quaid-I-Azam University, Islamabad, Pakistan
A. Ahmad, M.I. Asghar, A. Awais, M.I.M. Awan, M. Gul, H.R. Hoorani, W.A. Khan, M.A. Shah, M. Shoaib, M. Waqas

AGH University of Science and Technology Faculty of Computer Science, Electronics and Telecommunications, Krakow, Poland
V. Avati, L. Grzanka, M. Malawski

National Centre for Nuclear Research, Swierk, Poland
H. Bialkowska, M. Bluj, B. Boimska, M. Górski, M. Kazana, M. Szleper, P. Zalewski

Institute of Experimental Physics, Faculty of Physics, University of Warsaw, Warsaw, Poland
K. Bunkowski, K. Doroba, A. Kalinowski, M. Konecki, J. Krolikowski

Laboratório de Instrumentação e Física Experimental de Partículas, Lisboa, Portugal
M. Araujo, P. Bargassa, D. Bastos, A. Boletti, P. Faccioli, M. Gallinaro, J. Hollar, N. Leonardo, T. Niknejad, M. Pisano, J. Seixas, O. Toldaiev, J. Varela

Joint Institute for Nuclear Research, Dubna, Russia
S. Afanasiev, D. Budkouski, I. Golutvin, I. Gorbunov, V. Karjavine, V. Korenkov, A. Lanev, A. Malakhov, V. Matveev[58,59], V. Palichik, V. Perelygin, M. Savina, V. Shalaev, S. Shmatov, S. Shulha, V. Smirnov, O. Teryaev, N. Voytishin, B.S. Yuldashev[60], A. Zarubin, I. Zhizhin

Petersburg Nuclear Physics Institute, Gatchina (St. Petersburg), Russia
G. Gavrilov, V. Golovtcov, Y. Ivanov, V. Kim[61], E. Kuznetsova[62], V. Murzin, V. Oreshkin, I. Smirnov, D. Sosnov, V. Sulimov, L. Uvarov, S. Volkov, A. Vorobyev
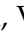
Institute for Nuclear Research, Moscow, Russia
Yu. Andreev, A. Dermenev, S. Gninenko, N. Golubev, A. Karneyeu, D. Kirpichnikov, M. Kirsanov, N. Krasnikov, A. Pashenkov, G. Pivovarov, A. Toropin

Moscow Institute of Physics and Technology, Moscow, Russia
T. Aushev

National Research Center 'Kurchatov Institute', Moscow, Russia
V. Epshteyn, V. Gavrilov, N. Lychkovskaya, A. Nikitenko[63], V. Popov, A. Stepennov, M. Toms, E. Vlasov, A. Zhokin

National Research Nuclear University 'Moscow Engineering Physics Institute' (MEPhI), Moscow, Russia
O. Bychkova, R. Chistov[64], M. Danilov[64], A. Oskin, P. Parygin, S. Polikarpov[64]

P.N. Lebedev Physical Institute, Moscow, Russia
V. Andreev, M. Azarkin, I. Dremin, M. Kirakosyan, A. Terkulov

Skobeltsyn Institute of Nuclear Physics, Lomonosov Moscow State University, Moscow, Russia
A. Belyaev, E. Boos, V. Bunichev, M. Dubinin[65], L. Dudko, A. Ershov, V. Klyukhin, O. Kodolova, I. Lokhtin, S. Obraztsov, M. Perfilov, S. Petrushanko, V. Savrin

Novosibirsk State University (NSU), Novosibirsk, Russia
V. Blinov[66], T. Dimova[66], L. Kardapoltsev[66], A. Kozyrev[66], I. Ovtin[66], O. Radchenko[66],

Y. Skovpen[66] (iD)

Institute for High Energy Physics of National Research Centre 'Kurchatov Institute', Protvino, Russia

I. Azhgirey (iD), I. Bayshev, D. Elumakhov, V. Kachanov, D. Konstantinov (iD), P. Mandrik (iD), V. Petrov, R. Ryutin, S. Slabospitskii (iD), A. Sobol, S. Troshin (iD), N. Tyurin, A. Uzunian, A. Volkov

National Research Tomsk Polytechnic University, Tomsk, Russia

A. Babaev, V. Okhotnikov
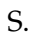
Tomsk State University, Tomsk, Russia

V. Borshch, V. Ivanchenko (iD), E. Tcherniaev (iD)

University of Belgrade: Faculty of Physics and VINCA Institute of Nuclear Sciences, Belgrade, Serbia

P. Adzic[67] (iD), M. Dordevic (iD), P. Milenovic (iD), J. Milosevic (iD)
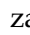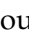
Centro de Investigaciones Energéticas Medioambientales y Tecnológicas (CIEMAT), Madrid, Spain

M. Aguilar-Benitez, J. Alcaraz Maestre (iD), A. Álvarez Fernández, I. Bachiller, M. Barrio Luna, Cristina F. Bedoya (iD), C.A. Carrillo Montoya (iD), M. Cepeda (iD), M. Cerrada, N. Colino (iD), B. De La Cruz, A. Delgado Peris (iD), J.P. Fernández Ramos (iD), J. Flix (iD), M.C. Fouz (iD), O. Gonzalez Lopez (iD), S. Goy Lopez (iD), J.M. Hernandez (iD), M.I. Josa (iD), J. León Holgado (iD), D. Moran, Á. Navarro Tobar (iD), C. Perez Dengra, A. Pérez-Calero Yzquierdo (iD), J. Puerta Pelayo (iD), I. Redondo (iD), L. Romero, S. Sánchez Navas, L. Urda Gómez (iD), C. Willmott
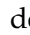
Universidad Autónoma de Madrid, Madrid, Spain

J.F. de Trocóniz

Universidad de Oviedo, Instituto Universitario de Ciencias y Tecnologías Espaciales de Asturias (ICTEA), Oviedo, Spain

B. Alvarez Gonzalez (iD), J. Cuevas (iD), J. Fernandez Menendez (iD), S. Folgueras (iD), I. Gonzalez Caballero (iD), J.R. González Fernández, E. Palencia Cortezon (iD), C. Ramón Álvarez, V. Rodríguez Bouza (iD), A. Soto Rodríguez, A. Trapote, N. Trevisani (iD), C. Vico Villalba

Instituto de Física de Cantabria (IFCA), CSIC-Universidad de Cantabria, Santander, Spain

J.A. Brochero Cifuentes (iD), I.J. Cabrillo, A. Calderon (iD), J. Duarte Campderros (iD), M. Fernandez (iD), C. Fernandez Madrazo (iD), P.J. Fernández Manteca (iD), A. García Alonso, G. Gomez, C. Martinez Rivero, P. Martinez Ruiz del Arbol (iD), F. Matorras (iD), P. Matorras Cuevas (iD), J. Piedra Gomez (iD), C. Prieels, A. Ruiz-Jimeno (iD), L. Scodellaro (iD), I. Vila, J.M. Vizan Garcia (iD)

University of Colombo, Colombo, Sri Lanka
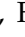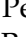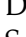
M.K. Jayananda, B. Kailasapathy[68], D.U.J. Sonnadara, D.D.C. Wickramarathna

University of Ruhuna, Department of Physics, Matara, Sri Lanka

W.G.D. Dharmaratna (iD), K. Liyanage, N. Perera, N. Wickramage

CERN, European Organization for Nuclear Research, Geneva, Switzerland

T.K. Aarrestad (iD), D. Abbaneo, J. Alimena (iD), E. Auffray, G. Auzinger, J. Baechler, P. Baillon[†], D. Barney (iD), J. Bendavid, M. Bianco (iD), A. Bocci (iD), C. Caillol, T. Camporesi, M. Capeans Garrido (iD), G. Cerminara, N. Chernyavskaya (iD), S.S. Chhibra (iD), S. Choudhury, M. Cipriani (iD), L. Cristella (iD), D. d'Enterria (iD), A. Dabrowski (iD), A. David (iD), A. De Roeck (iD), M.M. Defranchis (iD), M. Deile (iD), M. Dobson, M. Dünser (iD), N. Dupont, A. Elliott-Peisert, F. Fallavollita[69], A. Florent (iD), L. Forthomme (iD), G. Franzoni (iD), W. Funk, S. Ghosh (iD), S. Giani, D. Gigi, K. Gill, F. Glege, L. Gouskos (iD), E. Govorkova (iD), M. Haranko (iD), J. Hegeman (iD),

V. Innocente ⓘ, T. James, P. Janot ⓘ, J. Kaspar ⓘ, J. Kieseler ⓘ, M. Komm ⓘ, N. Kratochwil, C. Lange ⓘ, S. Laurila, P. Lecoq ⓘ, A. Lintuluoto, C. Lourenço ⓘ, B. Maier, L. Malgeri ⓘ, S. Mallios, M. Mannelli, A.C. Marini ⓘ, F. Meijers, S. Mersi ⓘ, E. Meschi ⓘ, F. Moortgat ⓘ, M. Mulders ⓘ, S. Orfanelli, L. Orsini, F. Pantaleo ⓘ, E. Perez, M. Peruzzi, A. Petrilli, G. Petrucciani ⓘ, A. Pfeiffer ⓘ, M. Pierini ⓘ, D. Piparo, M. Pitt ⓘ, H. Qu ⓘ, T. Quast, D. Rabady ⓘ, A. Racz, G. Reales Gutiérrez, M. Rovere, H. Sakulin, J. Salfeld-Nebgen ⓘ, S. Scarfi, C. Schwick, M. Selvaggi ⓘ, A. Sharma, P. Silva ⓘ, W. Snoeys ⓘ, P. Sphicas[70] ⓘ, S. Summers ⓘ, K. Tatar ⓘ, V.R. Tavolaro ⓘ, D. Treille, P. Tropea, A. Tsirou, J. Wanczyk[71], K.A. Wozniak, W.D. Zeuner
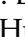
Paul Scherrer Institut, Villigen, Switzerland
L. Caminada[72] ⓘ, A. Ebrahimi ⓘ, W. Erdmann, R. Horisberger, Q. Ingram, H.C. Kaestli, D. Kotlinski, U. Langenegger, M. Missiroli[72] ⓘ, L. Noehte[72] ⓘ, T. Rohe

ETH Zurich - Institute for Particle Physics and Astrophysics (IPA), Zurich, Switzerland
K. Androsov[71] ⓘ, M. Backhaus ⓘ, P. Berger, A. Calandri ⓘ, A. De Cosa, G. Dissertori ⓘ, M. Dittmar, M. Donegà, C. Dorfer ⓘ, F. Eble, K. Gedia, F. Glessgen, T.A. Gómez Espinosa ⓘ, C. Grab ⓘ, D. Hits, W. Lustermann, A.-M. Lyon, R.A. Manzoni ⓘ, L. Marchese ⓘ, C. Martin Perez, M.T. Meinhard, F. Nessi-Tedaldi, J. Niedziela ⓘ, F. Pauss, V. Perovic, S. Pigazzini ⓘ, M.G. Ratti ⓘ, M. Reichmann, C. Reissel, T. Reitenspiess, B. Ristic ⓘ, D. Ruini, D.A. Sanz Becerra ⓘ, V. Stampf, J. Steggemann[71] ⓘ, R. Wallny ⓘ
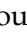
Universität Zürich, Zurich, Switzerland
C. Amsler[73] ⓘ, P. Bärtschi, C. Botta ⓘ, D. Brzhechko, M.F. Canelli ⓘ, K. Cormier, A. De Wit ⓘ, R. Del Burgo, J.K. Heikkilä ⓘ, M. Huwiler, W. Jin, A. Jofrehei ⓘ, B. Kilminster ⓘ, S. Leontsinis ⓘ, S.P. Liechti, A. Macchiolo ⓘ, P. Meiring, V.M. Mikuni ⓘ, U. Molinatti, I. Neutelings, A. Reimers, P. Robmann, S. Sanchez Cruz ⓘ, K. Schweiger ⓘ, M. Senger, Y. Takahashi ⓘ

National Central University, Chung-Li, Taiwan
C. Adloff[74], C.M. Kuo, W. Lin, A. Roy ⓘ, T. Sarkar[41] ⓘ, S.S. Yu

National Taiwan University (NTU), Taipei, Taiwan
L. Ceard, Y. Chao, K.F. Chen ⓘ, P.H. Chen ⓘ, P.s. Chen, H. Cheng ⓘ, W.-S. Hou ⓘ, Y.y. Li, R.-S. Lu, E. Paganis ⓘ, A. Psallidas, A. Steen, H.y. Wu, E. Yazgan ⓘ, P.r. Yu

Chulalongkorn University, Faculty of Science, Department of Physics, Bangkok, Thailand
B. Asavapibhop ⓘ, C. Asawatangtrakuldee ⓘ, N. Srimanobhas ⓘ

Çukurova University, Physics Department, Science and Art Faculty, Adana, Turkey
F. Boran ⓘ, S. Damarseckin[75], Z.S. Demiroglu ⓘ, F. Dolek ⓘ, I. Dumanoglu[76] ⓘ, E. Eskut, Y. Guler[77] ⓘ, E. Gurpinar Guler[77] ⓘ, C. Isik, O. Kara, A. Kayis Topaksu, U. Kiminsu ⓘ, G. Onengut, K. Ozdemir[78], A. Polatoz, A.E. Simsek ⓘ, B. Tali[79], U.G. Tok ⓘ, S. Turkcapar, I.S. Zorbakir ⓘ

Middle East Technical University, Physics Department, Ankara, Turkey
G. Karapinar, K. Ocalan[80] ⓘ, M. Yalvac[81] ⓘ

Bogazici University, Istanbul, Turkey
B. Akgun, I.O. Atakisi ⓘ, E. Gulmez ⓘ, M. Kaya[82] ⓘ, O. Kaya[83], Ö. Özçelik, S. Tekten[84], E.A. Yetkin[85] ⓘ

Istanbul Technical University, Istanbul, Turkey
A. Cakir ⓘ, K. Cankocak[76] ⓘ, Y. Komurcu, S. Sen[86] ⓘ

Istanbul University, Istanbul, Turkey
S. Cerci[79], I. Hos[87], B. Isildak[88], B. Kaynak, S. Ozkorucuklu, H. Sert (iD), C. Simsek, D. Sunar Cerci[79] (iD), C. Zorbilmez

Institute for Scintillation Materials of National Academy of Science of Ukraine, Kharkov, Ukraine
B. Grynyov

National Scientific Center, Kharkov Institute of Physics and Technology, Kharkov, Ukraine
L. Levchuk (iD)

University of Bristol, Bristol, United Kingdom
D. Anthony, E. Bhal (iD), S. Bologna, J.J. Brooke (iD), A. Bundock (iD), E. Clement (iD), D. Cussans (iD), H. Flacher (iD), M. Glowacki, J. Goldstein (iD), G.P. Heath, H.F. Heath (iD), L. Kreczko (iD), B. Krikler (iD), S. Paramesvaran, S. Seif El Nasr-Storey, V.J. Smith, N. Stylianou[89] (iD), K. Walkingshaw Pass, R. White

Rutherford Appleton Laboratory, Didcot, United Kingdom
K.W. Bell, A. Belyaev[90] (iD), C. Brew (iD), R.M. Brown, D.J.A. Cockerill, C. Cooke, K.V. Ellis, K. Harder, S. Harper, M.-L. Holmberg[91], J. Linacre (iD), K. Manolopoulos, D.M. Newbold (iD), E. Olaiya, D. Petyt, T. Reis (iD), T. Schuh, C.H. Shepherd-Themistocleous, I.R. Tomalin, T. Williams (iD)

Imperial College, London, United Kingdom
R. Bainbridge (iD), P. Bloch (iD), S. Bonomally, J. Borg (iD), S. Breeze, O. Buchmuller, V. Cepaitis (iD), G.S. Chahal[92] (iD), D. Colling, P. Dauncey (iD), G. Davies (iD), M. Della Negra (iD), S. Fayer, G. Fedi (iD), G. Hall (iD), M.H. Hassanshahi, G. Iles, J. Langford, L. Lyons, A.-M. Magnan, S. Malik, A. Martelli (iD), D.G. Monk, J. Nash[93] (iD), M. Pesaresi, B.C. Radburn-Smith, D.M. Raymond, A. Richards, A. Rose, E. Scott (iD), C. Seez, A. Shtipliyski, A. Tapper (iD), K. Uchida, T. Virdee[21] (iD), M. Vojinovic (iD), N. Wardle (iD), S.N. Webb (iD), D. Winterbottom

Brunel University, Uxbridge, United Kingdom
K. Coldham, J.E. Cole (iD), A. Khan, P. Kyberd (iD), I.D. Reid (iD), L. Teodorescu, S. Zahid (iD)

Baylor University, Waco, Texas, USA
S. Abdullin (iD), A. Brinkerhoff (iD), B. Caraway (iD), J. Dittmann (iD), K. Hatakeyama (iD), A.R. Kanuganti, B. McMaster (iD), M. Saunders (iD), S. Sawant, C. Sutantawibul, J. Wilson (iD)

Catholic University of America, Washington, DC, USA
R. Bartek (iD), A. Dominguez (iD), R. Uniyal (iD), A.M. Vargas Hernandez

The University of Alabama, Tuscaloosa, Alabama, USA
A. Buccilli (iD), S.I. Cooper (iD), D. Di Croce (iD), S.V. Gleyzer (iD), C. Henderson (iD), C.U. Perez (iD), P. Rumerio[94] (iD), C. West (iD)

Boston University, Boston, Massachusetts, USA
A. Akpinar (iD), A. Albert (iD), D. Arcaro (iD), C. Cosby (iD), Z. Demiragli (iD), C. Erice (iD), E. Fontanesi, D. Gastler, S. May (iD), J. Rohlf (iD), K. Salyer (iD), D. Sperka, D. Spitzbart (iD), I. Suarez (iD), A. Tsatsos, S. Yuan, D. Zou

Brown University, Providence, Rhode Island, USA
G. Benelli (iD), B. Burkle (iD), X. Coubez[23], D. Cutts (iD), M. Hadley (iD), U. Heintz (iD), J.M. Hogan[95] (iD), T. Kwon, G. Landsberg (iD), K.T. Lau (iD), D. Li, M. Lukasik, J. Luo (iD), M. Narain, N. Pervan, S. Sagir[96] (iD), F. Simpson, E. Usai (iD), W.Y. Wong, X. Yan (iD), D. Yu (iD), W. Zhang

University of California, Davis, Davis, California, USA

J. Bonilla, C. Brainerd, R. Breedon, M. Calderon De La Barca Sanchez, M. Chertok, J. Conway, P.T. Cox, R. Erbacher, G. Haza, F. Jensen, O. Kukral, R. Lander, M. Mulhearn, D. Pellett, B. Regnery, D. Taylor, Y. Yao, F. Zhang
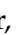
University of California, Los Angeles, California, USA

M. Bachtis, R. Cousins, A. Datta, D. Hamilton, J. Hauser, M. Ignatenko, M.A. Iqbal, T. Lam, W.A. Nash, S. Regnard, D. Saltzberg, B. Stone, V. Valuev

University of California, Riverside, Riverside, California, USA

Y. Chen, R. Clare, J.W. Gary, M. Gordon, G. Hanson, G. Karapostoli, O.R. Long, N. Manganelli, W. Si, S. Wimpenny, Y. Zhang

University of California, San Diego, La Jolla, California, USA

J.G. Branson, P. Chang, S. Cittolin, S. Cooperstein, D. Diaz, J. Duarte, R. Gerosa, L. Giannini, J. Guiang, R. Kansal, V. Krutelyov, R. Lee, J. Letts, M. Masciovecchio, F. Mokhtar, M. Pieri, B.V. Sathia Narayanan, V. Sharma, M. Tadel, F. Würthwein, Y. Xiang, A. Yagil

University of California, Santa Barbara - Department of Physics, Santa Barbara, California, USA

N. Amin, C. Campagnari, M. Citron, G. Collura, A. Dorsett, V. Dutta, J. Incandela, M. Kilpatrick, J. Kim, B. Marsh, H. Mei, M. Oshiro, M. Quinnan, J. Richman, U. Sarica, F. Setti, J. Sheplock, P. Siddireddy, D. Stuart, S. Wang

California Institute of Technology, Pasadena, California, USA

A. Bornheim, O. Cerri, I. Dutta, J.M. Lawhorn, N. Lu, J. Mao, H.B. Newman, T.Q. Nguyen, M. Spiropulu, J.R. Vlimant, C. Wang, S. Xie, Z. Zhang, R.Y. Zhu
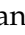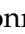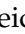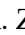
Carnegie Mellon University, Pittsburgh, Pennsylvania, USA

J. Alison, S. An, M.B. Andrews, P. Bryant, T. Ferguson, A. Harilal, C. Liu, T. Mudholkar, M. Paulini, A. Sanchez, W. Terrill
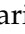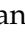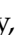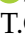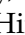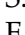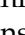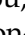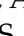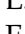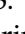
University of Colorado Boulder, Boulder, Colorado, USA

J.P. Cumalat, W.T. Ford, A. Hassani, G. Karathanasis, E. MacDonald, R. Patel, A. Perloff, C. Savard, N. Schonbeck, K. Stenson, K.A. Ulmer, S.R. Wagner, N. Zipper

Cornell University, Ithaca, New York, USA

J. Alexander, S. Bright-Thonney, X. Chen, Y. Cheng, D.J. Cranshaw, X. Fan, S. Hogan, J. Monroy, J.R. Patterson, D. Quach, J. Reichert, M. Reid, A. Ryd, W. Sun, J. Thom, P. Wittich, R. Zou

Fermi National Accelerator Laboratory, Batavia, Illinois, USA

M. Albrow, M. Alyari, G. Apollinari, A. Apresyan, A. Apyan, L.A.T. Bauerdick, D. Berry, J. Berryhill, P.C. Bhat, K. Burkett, J.N. Butler, A. Canepa, G.B. Cerati, H.W.K. Cheung, F. Chlebana, K.F. Di Petrillo, J. Dickinson, V.D. Elvira, Y. Feng, J. Freeman, A. Gandrakota, Z. Gecse, L. Gray, D. Green, S. Grünendahl, O. Gutsche, R.M. Harris, R. Heller, T.C. Herwig, J. Hirschauer, B. Jayatilaka, S. Jindariani, M. Johnson, U. Joshi, T. Klijnsma, B. Klima, K.H.M. Kwok, S. Lammel, D. Lincoln, R. Lipton, T. Liu, C. Madrid, K. Maeshima, C. Mantilla, D. Mason, P. McBride, P. Merkel, S. Mrenna, S. Nahn, J. Ngadiuba, V. Papadimitriou, N. Pastika, K. Pedro, C. Pena[65], F. Ravera, A. Reinsvold Hall[97], L. Ristori, E. Sexton-Kennedy, N. Smith, A. Soha, L. Spiegel, S. Stoynev, J. Strait, L. Taylor, S. Tkaczyk, N.V. Tran, L. Uplegger, E.W. Vaandering, H.A. Weber

University of Florida, Gainesville, Florida, USA

P. Avery, D. Bourilkov ⓘ, L. Cadamuro ⓘ, V. Cherepanov, R.D. Field, D. Guerrero, M. Kim, E. Koenig, J. Konigsberg ⓘ, A. Korytov, K.H. Lo, K. Matchev ⓘ, N. Menendez ⓘ, G. Mitselmakher ⓘ, A. Muthirakalayil Madhu, N. Rawal, D. Rosenzweig, S. Rosenzweig, K. Shi ⓘ, J. Wang ⓘ, Z. Wu ⓘ, E. Yigitbasi ⓘ, X. Zuo
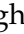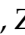
Florida State University, Tallahassee, Florida, USA

T. Adams ⓘ, A. Askew ⓘ, R. Habibullah ⓘ, V. Hagopian, K.F. Johnson, R. Khurana, T. Kolberg ⓘ, G. Martinez, H. Prosper ⓘ, C. Schiber, O. Viazlo ⓘ, R. Yohay ⓘ, J. Zhang

Florida Institute of Technology, Melbourne, Florida, USA

M.M. Baarmand ⓘ, S. Butalla, T. Elkafrawy[16] ⓘ, M. Hohlmann ⓘ, R. Kumar Verma ⓘ, D. Noonan ⓘ, M. Rahmani, F. Yumiceva ⓘ

University of Illinois at Chicago (UIC), Chicago, Illinois, USA

M.R. Adams, H. Becerril Gonzalez ⓘ, R. Cavanaugh ⓘ, S. Dittmer, O. Evdokimov ⓘ, C.E. Gerber ⓘ, D.J. Hofman ⓘ, A.H. Merrit, C. Mills ⓘ, G. Oh ⓘ, T. Roy, S. Rudrabhatla, M.B. Tonjes ⓘ, N. Varelas ⓘ, J. Viinikainen ⓘ, X. Wang, Z. Ye ⓘ
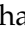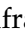
The University of Iowa, Iowa City, Iowa, USA

M. Alhusseini ⓘ, K. Dilsiz[98] ⓘ, L. Emediato, R.P. Gandrajula ⓘ, O.K. Köseyan ⓘ, J.-P. Merlo, A. Mestvirishvili[99], J. Nachtman, H. Ogul[100] ⓘ, Y. Onel ⓘ, A. Penzo, C. Snyder, E. Tiras[101] ⓘ

Johns Hopkins University, Baltimore, Maryland, USA

O. Amram ⓘ, B. Blumenfeld ⓘ, L. Corcodilos ⓘ, J. Davis, A.V. Gritsan ⓘ, S. Kyriacou, P. Maksimovic ⓘ, J. Roskes ⓘ, M. Swartz, T.Á. Vámi ⓘ

The University of Kansas, Lawrence, Kansas, USA

A. Abreu, J. Anguiano, C. Baldenegro Barrera ⓘ, P. Baringer ⓘ, A. Bean ⓘ, Z. Flowers, T. Isidori, S. Khalil ⓘ, J. King, G. Krintiras ⓘ, A. Kropivnitskaya ⓘ, M. Lazarovits, C. Le Mahieu, C. Lindsey, J. Marquez, N. Minafra ⓘ, M. Murray ⓘ, M. Nickel, C. Rogan ⓘ, C. Royon, R. Salvatico ⓘ, S. Sanders, E. Schmitz, C. Smith ⓘ, Q. Wang ⓘ, Z. Warner, J. Williams ⓘ, G. Wilson ⓘ

Kansas State University, Manhattan, Kansas, USA

S. Duric, A. Ivanov ⓘ, K. Kaadze ⓘ, D. Kim, Y. Maravin ⓘ, T. Mitchell, A. Modak, K. Nam
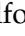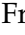
Lawrence Livermore National Laboratory, Livermore, California, USA

F. Rebassoo, D. Wright
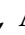
University of Maryland, College Park, Maryland, USA

E. Adams, A. Baden, O. Baron, A. Belloni ⓘ, S.C. Eno ⓘ, N.J. Hadley ⓘ, S. Jabeen ⓘ, R.G. Kellogg, T. Koeth, Y. Lai, S. Lascio, A.C. Mignerey, S. Nabili, C. Palmer ⓘ, M. Seidel ⓘ, A. Skuja ⓘ, L. Wang, K. Wong ⓘ

Massachusetts Institute of Technology, Cambridge, Massachusetts, USA

D. Abercrombie, G. Andreassi, R. Bi, W. Busza ⓘ, I.A. Cali, Y. Chen ⓘ, M. D'Alfonso ⓘ, J. Eysermans, C. Freer ⓘ, G. Gomez Ceballos, M. Goncharov, P. Harris, M. Hu, M. Klute ⓘ, D. Kovalskyi ⓘ, J. Krupa, Y.-J. Lee ⓘ, K. Long ⓘ, C. Mironov ⓘ, C. Paus ⓘ, D. Rankin ⓘ, C. Roland ⓘ, G. Roland, Z. Shi ⓘ, G.S.F. Stephans ⓘ, J. Wang, Z. Wang ⓘ, B. Wyslouch ⓘ

University of Minnesota, Minneapolis, Minnesota, USA

R.M. Chatterjee, A. Evans ⓘ, J. Hiltbrand, Sh. Jain ⓘ, B.M. Joshi ⓘ, M. Krohn, Y. Kubota, J. Mans ⓘ, M. Revering, R. Rusack ⓘ, R. Saradhy, N. Schroeder ⓘ, N. Strobbe ⓘ, M.A. Wadud

University of Nebraska-Lincoln, Lincoln, Nebraska, USA

K. Bloom, M. Bryson, S. Chauhan, D.R. Claes, C. Fangmeier, L. Finco, F. Golf, C. Joo, I. Kravchenko, I. Reed, J.E. Siado, G.R. Snow[†], W. Tabb, A. Wightman, F. Yan, A.G. Zecchinelli
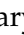
State University of New York at Buffalo, Buffalo, New York, USA

G. Agarwal, H. Bandyopadhyay, L. Hay, I. Iashvili, A. Kharchilava, C. McLean, D. Nguyen, J. Pekkanen, S. Rappoccio, A. Williams

Northeastern University, Boston, Massachusetts, USA

G. Alverson, E. Barberis, Y. Haddad, Y. Han, A. Hortiangtham, A. Krishna, J. Li, J. Lidrych, G. Madigan, B. Marzocchi, D.M. Morse, V. Nguyen, T. Orimoto, A. Parker, L. Skinnari, A. Tishelman-Charny, T. Wamorkar, B. Wang, A. Wisecarver, D. Wood

Northwestern University, Evanston, Illinois, USA

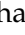S. Bhattacharya, J. Bueghly, Z. Chen, A. Gilbert, T. Gunter, K.A. Hahn, Y. Liu, N. Odell, M.H. Schmitt, M. Velasco
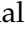
University of Notre Dame, Notre Dame, Indiana, USA

R. Band, R. Bucci, M. Cremonesi, A. Das, N. Dev, R. Goldouzian, M. Hildreth, K. Hurtado Anampa, C. Jessop, K. Lannon, J. Lawrence, N. Loukas, D. Lutton, J. Mariano, N. Marinelli, I. Mcalister, T. McCauley, C. Mcgrady, K. Mohrman, C. Moore, Y. Musienko[58], R. Ruchti, A. Townsend, M. Wayne, M. Zarucki, L. Zygala

The Ohio State University, Columbus, Ohio, USA

B. Bylsma, L.S. Durkin, B. Francis, C. Hill, M. Nunez Ornelas, K. Wei, B.L. Winer, B.R. Yates

Princeton University, Princeton, New Jersey, USA

F.M. Addesa, B. Bonham, P. Das, G. Dezoort, P. Elmer, A. Frankenthal, B. Greenberg, N. Haubrich, S. Higginbotham, A. Kalogeropoulos, G. Kopp, S. Kwan, D. Lange, D. Marlow, K. Mei, I. Ojalvo, J. Olsen, D. Stickland, C. Tully

University of Puerto Rico, Mayaguez, Puerto Rico, USA

S. Malik, S. Norberg
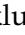
Purdue University, West Lafayette, Indiana, USA

A.S. Bakshi, V.E. Barnes, R. Chawla, S. Das, L. Gutay, M. Jones, A.W. Jung, D. Kondratyev, A.M. Koshy, M. Liu, G. Negro, N. Neumeister, G. Paspalaki, S. Piperov, A. Purohit, J.F. Schulte, M. Stojanovic[17], J. Thieman, F. Wang, R. Xiao, W. Xie

Purdue University Northwest, Hammond, Indiana, USA

J. Dolen, N. Parashar

Rice University, Houston, Texas, USA

D. Acosta, A. Baty, T. Carnahan, M. Decaro, S. Dildick, K.M. Ecklund, S. Freed, P. Gardner, F.J.M. Geurts, A. Kumar, W. Li, B.P. Padley, R. Redjimi, J. Rotter, W. Shi, A.G. Stahl Leiton, S. Yang, L. Zhang[102], Y. Zhang

University of Rochester, Rochester, New York, USA

A. Bodek, P. de Barbaro, R. Demina, J.L. Dulemba, C. Fallon, T. Ferbel, M. Galanti, A. Garcia-Bellido, O. Hindrichs, A. Khukhunaishvili, E. Ranken, R. Taus, G.P. Van Onsem

The Rockefeller University, New York, New York, USA

K. Goulianos

Rutgers, The State University of New Jersey, Piscataway, New Jersey, USA
B. Chiarito, J.P. Chou (ID), Y. Gershtein (ID), E. Halkiadakis (ID), A. Hart, M. Heindl (ID), O. Karacheban[25] (ID), I. Laflotte, A. Lath (ID), R. Montalvo, K. Nash, M. Osherson, S. Salur (ID), S. Schnetzer, S. Somalwar (ID), R. Stone, S.A. Thayil (ID), S. Thomas, H. Wang (ID)

University of Tennessee, Knoxville, Tennessee, USA
H. Acharya, A.G. Delannoy (ID), S. Fiorendi (ID), T. Holmes (ID), S. Spanier (ID)

Texas A&M University, College Station, Texas, USA
O. Bouhali[103] (ID), M. Dalchenko (ID), A. Delgado (ID), R. Eusebi, J. Gilmore, T. Huang, T. Kamon[104], H. Kim (ID), S. Luo (ID), S. Malhotra, R. Mueller, D. Overton, D. Rathjens (ID), A. Safonov (ID)

Texas Tech University, Lubbock, Texas, USA
N. Akchurin, J. Damgov, V. Hegde, K. Lamichhane, S.W. Lee (ID), T. Mengke, S. Muthumuni (ID), T. Peltola (ID), I. Volobouev, Z. Wang, A. Whitbeck

Vanderbilt University, Nashville, Tennessee, USA
E. Appelt (ID), S. Greene, A. Gurrola (ID), W. Johns, A. Melo, K. Padeken (ID), F. Romeo (ID), P. Sheldon (ID), S. Tuo, J. Velkovska (ID)

University of Virginia, Charlottesville, Virginia, USA
M.W. Arenton (ID), B. Cardwell, B. Cox (ID), G. Cummings (ID), J. Hakala (ID), R. Hirosky (ID), M. Joyce (ID), A. Ledovskoy (ID), A. Li, C. Neu (ID), C.E. Perez Lara (ID), B. Tannenwald (ID), S. White (ID)

Wayne State University, Detroit, Michigan, USA
N. Poudyal (ID)

University of Wisconsin - Madison, Madison, WI, Wisconsin, USA
S. Banerjee, K. Black (ID), T. Bose (ID), S. Dasu (ID), I. De Bruyn (ID), P. Everaerts (ID), C. Galloni, H. He, M. Herndon (ID), A. Herve, U. Hussain, A. Lanaro, A. Loeliger, R. Loveless, J. Madhusudanan Sreekala (ID), A. Mallampalli, A. Mohammadi, D. Pinna, A. Savin, V. Shang, V. Sharma (ID), W.H. Smith (ID), D. Teague, S. Trembath-Reichert, W. Vetens (ID)

†: Deceased
1: Now at TU Wien, Wien, Austria
2: Now at Institute of Basic and Applied Sciences, Faculty of Engineering, Arab Academy for Science, Technology and Maritime Transport, Alexandria, Egypt
3: Now at Université Libre de Bruxelles, Bruxelles, Belgium
4: Now at Universidade Estadual de Campinas, Campinas, Brazil
5: Now at Federal University of Rio Grande do Sul, Porto Alegre, Brazil
6: Now at The University of the State of Amazonas, Manaus, Brazil
7: Now at University of Chinese Academy of Sciences, Beijing, China
8: Now at Department of Physics, Tsinghua University, Beijing, China
9: Now at UFMS, Nova Andradina, Brazil
10: Now at Nanjing Normal University Department of Physics, Nanjing, China
11: Now at The University of Iowa, Iowa City, Iowa, USA
12: Now at National Research Center 'Kurchatov Institute', Moscow, Russia
13: Now at Joint Institute for Nuclear Research, Dubna, Russia
14: Now at Cairo University, Cairo, Egypt
15: Now at British University in Egypt, Cairo, Egypt
16: Now at Ain Shams University, Cairo, Egypt
17: Now at Purdue University, West Lafayette, Indiana, USA
18: Now at Université de Haute Alsace, Mulhouse, France

19: Now at Tbilisi State University, Tbilisi, Georgia
20: Now at Erzincan Binali Yildirim University, Erzincan, Turkey
21: Now at CERN, European Organization for Nuclear Research, Geneva, Switzerland
22: Now at University of Hamburg, Hamburg, Germany
23: Now at RWTH Aachen University, III. Physikalisches Institut A, Aachen, Germany
24: Now at Isfahan University of Technology, Isfahan, Iran
25: Now at Brandenburg University of Technology, Cottbus, Germany
26: Now at Forschungszentrum Jülich, Juelich, Germany
27: Now at Physics Department, Faculty of Science, Assiut University, Assiut, Egypt
28: Now at Karoly Robert Campus, MATE Institute of Technology, Gyongyos, Hungary
29: Now at Institute of Physics, University of Debrecen, Debrecen, Hungary
30: Now at Institute of Nuclear Research ATOMKI, Debrecen, Hungary
31: Now at Universitatea Babes-Bolyai - Facultatea de Fizica, Cluj-Napoca, Romania
32: Now at MTA-ELTE Lendület CMS Particle and Nuclear Physics Group, Eötvös Loránd University, Budapest, Hungary
33: Now at Faculty of Informatics, University of Debrecen, Debrecen, Hungary
34: Now at Wigner Research Centre for Physics, Budapest, Hungary
35: Now at IIT Bhubaneswar, Bhubaneswar, India
36: Now at Institute of Physics, Bhubaneswar, India
37: Now at Punjab Agricultural University, Ludhiana, India
38: Now at UPES - University of Petroleum and Energy Studies, Dehradun, India
39: Now at Shoolini University, Solan, India
40: Now at University of Hyderabad, Hyderabad, India
41: Now at University of Visva-Bharati, Santiniketan, India
42: Now at Indian Institute of Science (IISc), Bangalore, India
43: Now at Indian Institute of Technology (IIT), Mumbai, India
44: Now at Deutsches Elektronen-Synchrotron, Hamburg, Germany
45: Now at Department of Physics, Isfahan University of Technology, Isfahan, Iran
46: Now at Sharif University of Technology, Tehran, Iran
47: Now at Department of Physics, University of Science and Technology of Mazandaran, Behshahr, Iran
48: Now at INFN Sezione di Bari, Università di Bari, Politecnico di Bari, Bari, Italy
49: Now at Italian National Agency for New Technologies, Energy and Sustainable Economic Development, Bologna, Italy
50: Now at Centro Siciliano di Fisica Nucleare e di Struttura Della Materia, Catania, Italy
51: Now at Scuola Superiore Meridionale, Università di Napoli Federico II, Napoli, Italy
52: Now at Università di Napoli 'Federico II', Napoli, Italy
53: Now at Consiglio Nazionale delle Ricerche - Istituto Officina dei Materiali, Perugia, Italy
54: Now at Riga Technical University, Riga, Latvia
55: Now at Department of Applied Physics, Faculty of Science and Technology, Universiti Kebangsaan Malaysia, Bangi, Malaysia
56: Now at Consejo Nacional de Ciencia y Tecnología, Mexico City, Mexico
57: Now at IRFU, CEA, Université Paris-Saclay, Gif-sur-Yvette, France
58: Now at Institute for Nuclear Research, Moscow, Russia
59: Now at National Research Nuclear University 'Moscow Engineering Physics Institute' (MEPhI), Moscow, Russia
60: Now at Institute of Nuclear Physics of the Uzbekistan Academy of Sciences, Tashkent, Uzbekistan
61: Now at St. Petersburg Polytechnic University, St. Petersburg, Russia

62: Now at University of Florida, Gainesville, Florida, USA
63: Now at Imperial College, London, United Kingdom
64: Now at P.N. Lebedev Physical Institute, Moscow, Russia
65: Now at California Institute of Technology, Pasadena, California, USA
66: Now at Budker Institute of Nuclear Physics, Novosibirsk, Russia
67: Now at Faculty of Physics, University of Belgrade, Belgrade, Serbia
68: Now at Trincomalee Campus, Eastern University, Sri Lanka, Nilaveli, Sri Lanka
69: Now at INFN Sezione di Pavia, Università di Pavia, Pavia, Italy
70: Now at National and Kapodistrian University of Athens, Athens, Greece
71: Now at Ecole Polytechnique Fédérale Lausanne, Lausanne, Switzerland
72: Now at Universität Zürich, Zurich, Switzerland
73: Now at Stefan Meyer Institute for Subatomic Physics, Vienna, Austria
74: Now at Laboratoire d'Annecy-le-Vieux de Physique des Particules, IN2P3-CNRS, Annecy-le-Vieux, France
75: Now at Şırnak University, Sirnak, Turkey
76: Now at Near East University, Research Center of Experimental Health Science, Nicosia, Turkey
77: Now at Konya Technical University, Konya, Turkey
78: Now at Piri Reis University, Istanbul, Turkey
79: Now at Adiyaman University, Adiyaman, Turkey
80: Now at Necmettin Erbakan University, Konya, Turkey
81: Now at Bozok Universitetesi Rektörlügü, Yozgat, Turkey
82: Now at Marmara University, Istanbul, Turkey
83: Now at Milli Savunma University, Istanbul, Turkey
84: Now at Kafkas University, Kars, Turkey
85: Now at Istanbul Bilgi University, Istanbul, Turkey
86: Now at Hacettepe University, Ankara, Turkey
87: Now at Istanbul University - Cerrahpasa, Faculty of Engineering, Istanbul, Turkey
88: Now at Ozyegin University, Istanbul, Turkey
89: Now at Vrije Universiteit Brussel, Brussel, Belgium
90: Now at School of Physics and Astronomy, University of Southampton, Southampton, United Kingdom
91: Now at Rutherford Appleton Laboratory, Didcot, United Kingdom
92: Now at IPPP Durham University, Durham, United Kingdom
93: Now at Monash University, Faculty of Science, Clayton, Australia
94: Now at Università di Torino, Torino, Italy
95: Now at Bethel University, St. Paul, Minneapolis, USA
96: Now at Karamanoğlu Mehmetbey University, Karaman, Turkey
97: Now at United States Naval Academy, Annapolis, N/A, USA
98: Now at Bingol University, Bingol, Turkey
99: Now at Georgian Technical University, Tbilisi, Georgia
100: Now at Sinop University, Sinop, Turkey
101: Now at Erciyes University, Kayseri, Turkey
102: Now at Institute of Modern Physics and Key Laboratory of Nuclear Physics and Ion-beam Application (MOE) - Fudan University, Shanghai, China
103: Now at Texas A&M University at Qatar, Doha, Qatar
104: Now at Kyungpook National University, Daegu, Korea